Establishment of Cyclodextrin-Based Hyperbranched Nanoparticles for Delivering Alpha Mangotin in Cancer Treatment

PhD. Student: Doan Thi Hong Van

Supervisor: Prof. Kazuo Sakurai

The University of Kitakyushu

Acknowledgement

To complete this doctoral dissertation, I would like to express my deep and sincere gratitude to my supervisor, Prof. Sakurai K., for giving me an invaluable opportunity to study in Japan, to do research and to change my world view. He provided guidance throughout this research, helped me improve my weakness. It was a great privilege and honor to work and study under his guidance. I am extremely grateful to Dr. Fujii S. for his advice and empathy. He has taught me the methodology to carry out the research and to present the research works as clearly as possible. I learned a lot of things from him such as how to think, how to study and how to deal with obstacles. His dynamism, vision and motivation have deeply inspired me. I also would like to thank Prof. Nakazawa K. for allowing me to learn spheroid cultivation in his laboratory. Special thanks are extended to Dr. Takahashi R. for helping me become more careful when writing papers and emails. I would like to express my love to all members of Sakurai Laboratory, Nakazawa Laboratory, Akiba Laboratory and Mochizuki Laboratory for their kindness.

I would like to thank all my Vietnamese friends in Hibikino campus, especially my roommate PhD student Nguyen K. L., for their supports and sharing their passion.

To my home country with all my love, I appreciate my family and my ex-supervisor for their hearty supports.

June, 2020

Doan Thi Hong Van

Table of Contents

Chapter I: Introduction

I. 1 General introduction

Plants not only plays a key role in regulating climate on the Earth but also have a great meaning for human existence. They have provided foods and medicines for human in prehistoric times. Through the 20th and into the 21st century, plants have been the major source of drugs. They produce various bioactive compounds to defend themselves against insects, bacteria, and herbivorous animals. Nowadays, plant natural products have become more attractive because it can be used as plant-based therapies and botanical healthcare products [1]. Many studies showed plant natural products display interesting bio/pharmacological activities including anticancer activities. According to the US National Cancer Institute, out of the 3000 plants identified as active against cancer, approximately 70% of the plants that have been identified active against cancer are tropical plant origin [2]. With development of solvent-extraction technology and analytical chemistry, anticancer drugs are extracted from tropical plants that have been available in large extent and caused to commercialize many plant-derived drugs.

I. 2 Alpha mangostin (MGS)

Among plant natural products, there is a xanthone derivative called α-mangostin (denoted as MGS hereinafter, see Figure 1-1) which can be extracted from the pericarps of natural fruit mangosteen [3]. Xanthone derivatives are known to exhibit diverse bioactivities depending on the modified structure on the three-membered heterocyclic ring [3-7]. MGS exhibits several bioactive properties such as antioxidant [8], cytotoxic [9], anti-inflammatory [10,11], antibacterial [9]. Besides, MGS is also highly expected as a candidate of anticancer drugs [12]. Its chemical structure has three phenolic hydroxy groups that are expected to capture reactive oxygen species (ROS) or donate protons, although this is not as effective as dihydroquinones in terms of the ability of ROS scavenger. It is also suggested its reduction of ROS in biological systems is probably mediated by its modulatory effect on the activity of glutathione peroxidase [10]. However, there are still gaps to biochemically connect the chemical structure of MGS and its bioactivities; nonetheless, it is certain that the nature of MGS antioxidation is closely related to its bioactivities.

In regard to biological pathways of MGS in cancer cell, Akao et al reported that MGS induces the down-regulation of signaling cascades involving mitogen-activated protein

(MAP) kinases and serine/threonine kinase (Akt) in human colon cancer DLD-1 cell [12]. MAP kinases play an important role in the cellular response to osmotic stress, ROS, heat shock and proinflammatory cytokines. They regulate proliferation, gene expression, differentiation, and mitosis, among others [13]. Akt (also known as protein kinase B) is involved in many cellular responses such as glucose metabolism, apoptosis, cell proliferation, transcription, and cell migration. Additionally, Akt is overexpressed in many cancer cells and is a good target to treat them [13]. MGS was found to have an effect of preventing cancer in a rat carcinogenesis bioassay and enhanced NK cell activity in a mouse model. Furthermore, it has been reported that MGS can act against cancers through inhibiting the fatty acid pathway. Therefore, MGS has great potential as an anticancer drug.

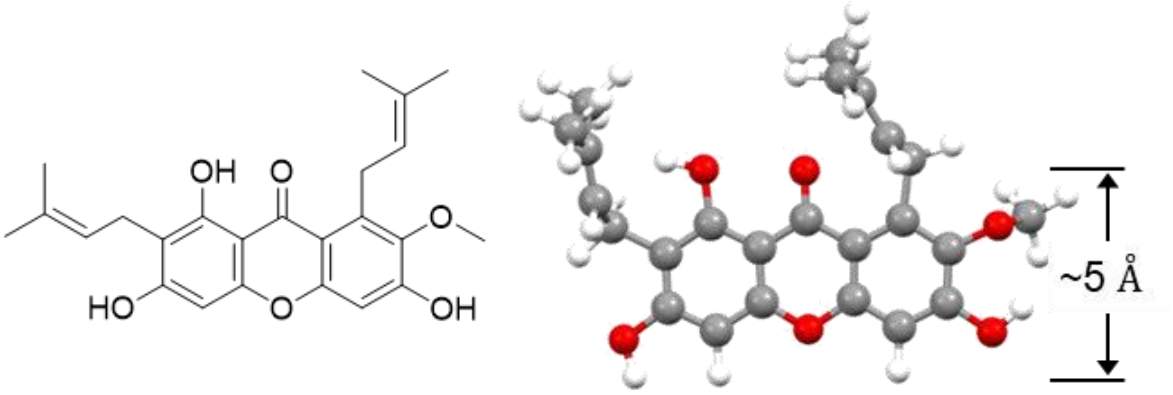

Figure 1-1. Chemical structure of MGS and its molecular model calculated with MOPAC.

However, the medical application of MGS is obstructed by its poor bioavailability. Bioavailability is the term used in the pharmaceutical field to describe the extent and rate at which a drug enters systemic circulation, thereby accessing the site of activity. This poor bioavailability of MGS is due to its very low solubility in water (2×10^{-4} mg/L) [14], compared with that of normal commercially available drugs (about at least ~ 10^{-3} g/L. Despite the presence of 10% ethanol, the solubility of MGS still made no significant improvement [15]. This issue presents a challenge for dissolving a large amount of this compound in an *in vivo* experiment.

I. 3 Drug delivery system (DDS)

A drug delivery system (DDS) is defined as a device that enables to introduce a therapeutic substance in the body [16]. DDS improves its efficacy and safety by controlling the rate, time, and place of release of drugs in the body. It can be designed properly for diverse

types of administration routes (i.e. oral, parenteral, nasal), specific targeted systems (i.e. antibody-targeted systems, receptor-mediated targeted delivery), delivering various of molecules even biomacromolecules. Thus, DDS has a tremendous impact on medicine. In addition to novel carriers for drug delivery such as collagen, microspheres, glass-like sugar matrices, nanotechnology-based drug delivery is considered to be the most important and popular due to its ability of integration into the human body [16]. The use of selective functional groups creates desirable internal signaling and helps nanoparticles be directed to an organ, tissue, or tumor without external control [17]. Due to uniform physicochemical and its nanosize (10^{-9} m), nanoparticle drug delivery system become a useful technique for delivering drug to specific target at intermolecular scale, overcoming the limitation of drugs (i.e., poor solubility).

For many anti-cancer drugs including DOX, THP, and mitomycin C, there are similar problems associated with their hydrophobicity. Because of such hydrophobicity, they are easily trapped by the cellular matrix and thus become widely distributed to normal organs as well as the tumor [18]. These drugs usually do not remain in the tumor for more than 10 min [19] and the extent to which they are distributed into cancerous regions is normally quite low. Consequences of this lack of tumor selectivity include insufficient therapeutic benefits and severe systemic toxicity [18]. Maeda et al. were the first to propose that, when these drugs are incorporated into particles with a suitable size, they accumulate in the tumor. When the particle size is adjusted to within a suitable range [20] (normally 10–100 nm in diameter), the particles circulate for longer in the blood by evading clearance by the mononuclear phagocytes in the liver and bypassing the filtration in the kidneys. Ultimately, a longer circulation time leads to drug accumulation at tissue sites affected by cancer. The endothelial lining of a tumor is incomplete and the tumor vasculature usually has large pores (0.1–2 μm in diameter) [21] because of the absence of vasculature-supporting tissues. These pores lead to leaky vessels forming, and are a reason for the permeability of tumors being higher than that of normal tissues. Once the nanoparticles enter the tumor region after penetrating the endothelial barrier, they may penetrate further into the interior of the tumor by diffusion or hydrophobic interaction with the cellular membrane. Since there is no lymphatic clearance of a tumor, the accumulated particles are retained within it. This phenomenon is called the enhanced permeation and retention effect (EPR effect) [22,23], which is the basic route of entry of all DDS that have been developed for antitumor therapy. Nakamura et al. showed

that N-(2-hydroxypropyl)methacrylamide copolymer containing groups (PHPMA) conjugated with THP was much better than THP itself. Specifically, they described that PHPMA-THP penetrated more efficiently into tumor-cell spheroids, had much better antitumor activity in an *in vivo* experiment, and showed a 4–20-times-higher concentration of drug in tumor tissue [24,25].

To overcome the limited solubility of MGS, the nanoparticle formulation strategy has been studied [26]. Verma et al. showed that MGS-encapsulated PLGA [poly(D,L-lactic-co-glycolic acid)] nanoparticles inhibited the growth, development, and metastasis of pancreatic cancer [27]. In addition, Yostawonkul et al. concluded that their nanocarrier-mediated delivery of MGS reduced the levels of pro-inflammatory mediators and may have utility in the non-surgical castration of male animals [28]. Although these were useful findings, the experiments mostly involved investigations only *in vitro* or *ex vivo*.

In our group, based on EPR effect, we investigated a common way which MGS was conjugated with N-(2-Hydroxypropyl)methacrylamide copolymer containing hydrazide groups (PHPMA). After attaching carbonyl groups into MGS structure to introduce PHPMA, MGS lost its cytotoxicity *in vitro* experiment. In present study, we propose a novel nanoparticle that enables to deliver MGS effectively in both *in vitro* and *in vivo* experiment.

I. 4 Cyclodextrin and its applications

As mentioned above, there are two main problems that limit on clinical use of MGS: one is the poor water-solubility of MGS, the other is small molecule. In order to improve these impediments, we choose cyclodextrins (CDs). It has been proved that CDs are biocompatible molecules approved by FDA as the material that can be injected into the human body and have already been used for a long time [29]. CD have a macro-cyclic structure made of 6, 7 or 8 units of glucose linked together, which is named as α, β or γCD, respectively. Since many hydroxyl groups are attached to the top and bottom of the molecule, it exhibits good water solubility, while the inside of the cyclic structure is hydrophobic and can contain hydrophobic molecules [30] which is called “molecular pocket” [30-32]. The cavity size is determined by the number of glucose units, and the cavity diameter of α, β and γCD is approximately 5.7, 7.8 and 9.5 Å, respectively (shown in Figure 1-2) [33,34]. This molecular pocket of CD can be used to capture hydrophobic drugs without damaging their

bioactivity [35,36]. Therefore, CDs can be used a building block for DDS and become our interest in this study.

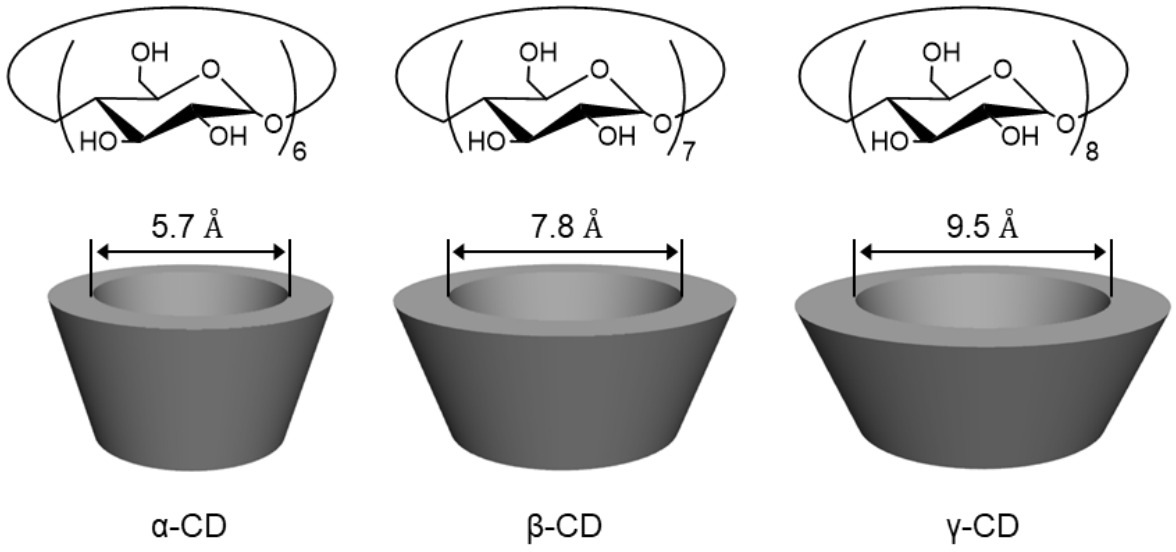

Figure 1-2. The chemical structure of α, β, and γCD and their schematic structures.

CDs are one of industrially useful compounds because of low cost and environmentally friendly. Furthermore, once CDs are incorporated into polymeric system, sometimes the cyclodextrin based polymeric materials exhibit excellent adsorption capacities for different kinds of compounds including hydrophobic organic compounds, dyes, and metal ions [37]. CD-based polymers have been used for biomedical application such as cancer imaging, therapy and theranostics [38]. Interestingly, those performance is better than original CDs and such a phenomenon is called "expanded pocket due to polymeric effect" [37]. Rungnim et al. have demonstrated the formation of the inclusion complex of βCD/MGS by both experimental and theoretical studies, which investigated the effect of ethanol as a co-solvent on the βCD/MGS formation [15]. As a first inclusion complex of βCD/MGS in polymer system, Phunpee et al. prepared chitosan bearing βCD and showed a potential as a carrier of MGS [39].

Among many CD-based nanoparticles (CDNPs), a CD-containing hyperbranched polymer prepared via polyaddition reaction between CD and epichlorohydrin (ECH) is capable of incorporating many CDs into the polymer. This synthesis method is a very simple, and the nanoparticles are expected for practical applications [40].

I. 5 Outline of thesis

In this thesis, we create cyclodextrin-based hyperbranched nanoparticles (CDNPs) that their size is suitable for using EPR effect in order to solve two main problems of MGS. Thus, the aims of this work are (i) enhance the solubility of MGS in aqueous solution; in other words, CDNP was expected to enable to encapsulate MGS; (ii) CDNP containing MGS shows anticancer efficacy.

Chapter II following this introductory chapter presents synthesis and characterization of cyclodextrin based-hyperbranched nanoparticles by dynamic and static light scattering (DLS and SLS) measurements. In Chapter III, we investigate the ability of encapsulating MGS in aqueous solution, explore the interaction of CD and MGS as well as monitor drug release of MGS from CDNPs. Chapter IV presents anticancer efficacy of nanoparticle encapsulating MGS through *in vitro* and *in vivo* experiment. This thesis ends with Chapter V, which summarizes all major findings and conclusions derived.

References

1 Che CT and Zhang H. Plant Natural Products for Human Health. Int J Mol Sci. 2019. 20: 830-34. 10.3390/ijms20040830.

2 Saurabh P, Paul NS and Amitha KH. Review of Procedures Used for the Extraction of Anti-Cancer Compounds from Tropical Plants. Anti-Cancer Agents in Medicinal Chemistry. 2015; 15: 314-26.

3 Pinto MMM, Sousa ME and Nascimento MSJ. Xanthone Derivatives: New Insights in Biological Activities. Curr Med Chem. 2005. 12: 2517-38.

4 Lin C-N, Liou S-J, Lee T-H, Chuang Y-C and Won S-J. Xanthone Derivatives as Potential Anti-cancer Drugs. Journal of Pharmacy and Pharmacology. 1996. 48: 539-44.

5 Han AR, Kim JA, Lantvit DD, Kardono LB, Riswan S, Chai H, Carcache de Blanco EJ, Farnsworth NR, Swanson SM and Kinghorn AD. Cytotoxic xanthone constituents of the stem bark of Garcinia mangostana (mangosteen). Journal of natural products. 2009; 72: 2028-31. 10.1021/np900517h.

6 Pedro M, Cerqueira F, Sousa ME, São M, Nascimentoa J and Pintoa M. Xanthones as Inhibitors of Growth of Human Cancer Cell Lines and Their Effects on the Proliferation of Human Lymphocytes In Vitro. Bioorg Med Chem. 2002. 10: 3725-30.

7 Na Y. Recent cancer drug development with xanthone structures. J Pharm Pharmacol. 2009; 61: 707-12. 10.1211/jpp/61.06.0002.

8 Jung H-A, Su B-N, Keller WJ, Mehta RG and Kinghorn AD. Antioxidant xanthones from the pericarp of *Garcinia mangostana* (Mangosteen). Journal of Agricultural and Food Chemistry. 2006. 54: 2077-82.

9 Pedraza-Chaverri J, Cardenas-Rodriguez N, Orozco-Ibarra M and Perez-Rojas JM. Medicinal properties of mangosteen (*Garcinia mangostana*). Food and Chem Toxicology. 2008; 46: 3227-39. 10.1016/j.fct.2008.07.024.

10 Janhom P and Dharmasaroja P. Neuroprotective Effects of Alpha-Mangostin on MPP(+)-Induced Apoptotic Cell Death in Neuroblastoma SH-SY5Y Cells. Journal of toxicology. 2015; 2015: 1-11. 10.1155/2015/919058.

11 Nakatania K, Nakahatab N, Arakawac T, Yasuda H and Ohizumia Y. Inhibiton of cyclooxygenase and prostaglandin E2 synthesis by γ-MGS, a xanthone dervative in mangosteen, in C6 rat glioma cell. Biochemical Pharmacology. 2002. 63: 73-79.

12 Akao Y , Nakagawa Y, Iinuma M and Nozawa Y. Anti-Cancer Effects of Xanthones from Pericarps of Mangosteen. Int J Mol Sci. 2008. 9: 355-70.

13 Tokunaga E, Oki E, Egashira A, Sadanaga N, Morita M, Kakeji Y and Maehara Y. Deregulation of the Akt Pathaway in Human Cancer Curr. Cancer Drug Targets. 2008. 8: 27-36.

14 National Center for Biotechnology Information. PubChem Database. alpha-Mangostin,https://pubchem.ncbi.nlm.nih.gov/compound/alpha-Mangostin

15 Rungnim C, Phunpee S, Kunaseth M, Namuangruk S, Rungsardthong K, Rungrotmongkol T and Ruktanonchai U. Co-solvation effect on the binding mode of

the alpha-mangostin/beta-cyclodextrin inclusion complex. Beilstein J Org Chem. 2015; 11: 2306-17. 10.3762/bjoc.11.251.

16 KJ Kewal. in *Methods in Molecular Biology* Vol. 437 (ed Kewal K. Jain) Ch. 1, 1-50 (Humana Press, Totowa, NJ, 2009).

17 Singh AK. Structure, Synthesis, and Application of Nanoparticles. 2016: 19-76. 10.1016/b978-0-12-801406-6.00002-9.

18 Maeda H, Nakamura H and Fang J. The EPR effect for macromolecular drug delivery to solid tumors: Improvement of tumor uptake, lowering of systemic toxicity, and distinct tumor imaging *in vivo*. Advanced drug delivery reviews. 2013. 65: 71-9. 10.1016/j.addr.2012.10.002.

19 Maeda H. Tumor-Selective Delivery of Macromolecular Drugs via the EPR Effect: Background and Future Prospects. Bioconjugate Chem. 2010. 21: 797-802.

20 Cabral H, Matsumoto Y, Mizuno K, Chen Q, Murakami M, Kimura M, Terada Y, Kano M R, Miyazono K, Uesaka M, Nishiyama N and Kataoka K. Accumulation of sub-100 nm polymeric micelles in poorly permeable tumours depends on size. Nat Nanotechnol. 2011. 6: 815-23. 10.1038/nnano.2011.166.

21 Kalyane D, Raval N, Maheshwari R, Tambe V, Kalia K and Tekade RK. Employment of enhanced permeability and retention effect (EPR): Nanoparticle-based precision tools for targeting of therapeutic and diagnostic agent in cancer. Mater Sci Eng C Mater Biol Appl. 2019. 98: 1252-76. 10.1016/j.msec.2019.01.066.

22 Maeda H, Wu J, Sawa T, Matsumura Y and Hori K. Tumor vascular permeability and the EPR effect in macromolecular therapeutics: a review. J Control Release. 2000. 65: 271–84.

23 Maeda H, Tsukigawa K and Fang J. A Retrospective 30 Years After Discovery of the Enhanced Permeability and Retention Effect of Solid Tumors: Next-Generation Chemotherapeutics and Photodynamic Therapy-Problems, Solutions, and Prospects. Microcirculation. 2016. 23: 173-82. 10.1111/micc.12228.

24 Nakamura H, Etrych T, Chytil P, Ohkubo M, Fang J, Ulbrich K and Maeda H. Two step mechanisms of tumor selective delivery of N-(2-hydroxypropyl)methacrylamide copolymer conjugated with pirarubicin via an acid-cleavable linkage. J Control Release. 2014. 174: 81-7. 10.1016/j.jconrel.2013.11.011.

25 Nakamura H, Koziolova E, Chytil P, Etrych T, Haratake M and Maeda H. Superior Penetration and Cytotoxicity of HPMA Copolymer Conjugates of Pirarubicin in Tumor Cell Spheroid. Mol Pharm. 2019. 16: 3452-59. 10.1021/acs.molpharmaceut.9b00248.

26 Wathoni N, Rusdin A, Motoyama K, Joni IM, Lesmana R and Muchtaridi M. Nanoparticle Drug Delivery Systems for alpha-Mangostin. Nanotechnol Sci Appl. 2020. 13: 23-36. 10.2147/NSA.S243017.

27 Verma RK, Yu W, Shrivastava A, Shankar S and Srivastava RK. alpha-Mangostin-encapsulated PLGA nanoparticles inhibit pancreatic carcinogenesis by targeting cancer stem cells in human, and transgenic (Kras(G12D), and Kras(G12D)/tp53R270H) mice. Sci Rep. 2016. 6: 32743. 10.1038/srep32743.

28 Yostawonkul J, Surassmo S, Namdee K, Khongkow M, Boonthum C, Pagseesing S, Saengkrit N, Ruktanonchai UR, Chatdarong K, Ponglowhapan S and Yata T. Nanocarrier-mediated delivery of alpha-mangostin for non-surgical castration of male animals. Sci Rep. 2017; 7: 16234-41. 10.1038/s41598-017-16563-3.

29 He Y, Fu P, Shen X and Gao H. Cyclodextrin-based aggregates and characterization by microscopy. Micron. 2008; 39: 495-516. 10.1016/j.micron.2007.06.017.

30 Gidwani B and Vyas A. A Comprehensive Review on Cyclodextrin-Based Carriers for Delivery of Chemotherapeutic Cytotoxic Anticancer Drugs. Biomed. Res. Int. 2015. 2015: 198-268. 10.1155/2015/198268.

31 Collins CJ, McCauliff LA, Hyun SH, Zhang Z, Paul LN, Kulkarni A, Zick K, Wirth M, Storch J and Thompson DH. Synthesis, characterization, and evaluation of pluronic-based beta-cyclodextrin polyrotaxanes for mobilization of accumulated cholesterol from Niemann-Pick type C fibroblasts. Biochemistry. 2013; 52: 3242-53. 10.1021/bi3010889.

32 Zhang J and Ma PX. Cyclodextrin-based supramolecular systems for drug delivery: recent progress and future perspective. Advanced drug delivery reviews. 2013; 65: 1215-33. 10.1016/j.addr.2013.05.001.

33 Simoes SM, Rey-Rico A, Concheiro A and Alvarez-Lorenzo C. Supramolecular cyclodextrin-based drug nanocarriers. Chemical communications. 2015; 51: 6275-89. 10.1039/c4cc10388b.

34 Wei H and Yu CY. Cyclodextrin-functionalized polymers as drug carriers for cancer therapy. Biomaterials science. 2015; 3: 1050-60. 10.1039/c4bm00417e.

35 Ammar HO, Salama HA, Ghorab M and Mahmoud AA. Formulation and biological evaluation of glimepiride-cyclodextrin-polymer systems. International journal of pharmaceutics. 2006; 309: 129-38. 10.1016/j.ijpharm.2005.11.024.

36 Ozdemir N and Erkin J. Enhancement of dissolution rate and bioavailability of sulfamethoxazole by complexation with beta-cyclodextrin. Drug development and industrial pharmacy. 2012; 38: 331-40. 10.3109/03639045.2011.604327.

37 Qin X, Bai L, Tan Y, Li L, Song F and Wang Y. β-Cyclodextrin-crosslinked polymeric adsorbent for simultaneous removal and stepwise recovery of organic dyes and heavy metal ions: Fabrication, performance and mechanisms. Chem Eng. 2019. 372: 1007-18. 10.1016/j.cej.2019.05.006.

38 Yao X, Huang P and Nie Z. Cyclodextrin-based polymer materials: From controlled synthesis to applications. Progress in Polymer Science. 2019. 93: 1-35. 10.1016/j.progpolymsci.2019.03.004.

39 Phunpee S, Suktham K, Surassmo S, Jarussophon S, Rungnim C, Soottitantawat A, Puttipipatkhachorn S and Ruktanonchai UR. Controllable encapsulation of alpha-mangostin with quaternized beta-cyclodextrin grafted chitosan using high shear mixing. International journal of pharmaceutics. 2018; 538: 21-29. 10.1016/j.ijpharm.2017.12.016.

40 Renard E, Deratani A, Volet G and Sebille B. Preparation and characterization of water soluble high molecular weight β-cyclodextrin-epichlorohydrin polymers. European Polymer Journal. 1997. 33: 49-57.

Chapter II: Synthesis and characterization of Cyclodextrin-based hyperbranched nanoparticles (CDNPs)

II. 1 Introduction

This chapter begins describing synthesis procedure of cyclodextrin-based hyperbranched nanoparticles (CDNPs). The synthesis procedure of CDNP was similar to the reported method in Renard et al study [1]. In a basic condition of pH = 13, the hydroxyl group in CDs are activated and reacted with the 1 or 3 carbon of ECH. When one carbon is nucleophilically attacked, new OH group is created and continues the reaction, resulting in formation of a hyperbranched polymer including CDs (Figure 2-1). This reaction mechanism means that the feeding weight ratio of ECH to CD (ECH/CD) is an important factor in controlling the molecular weight and the particle size [2].

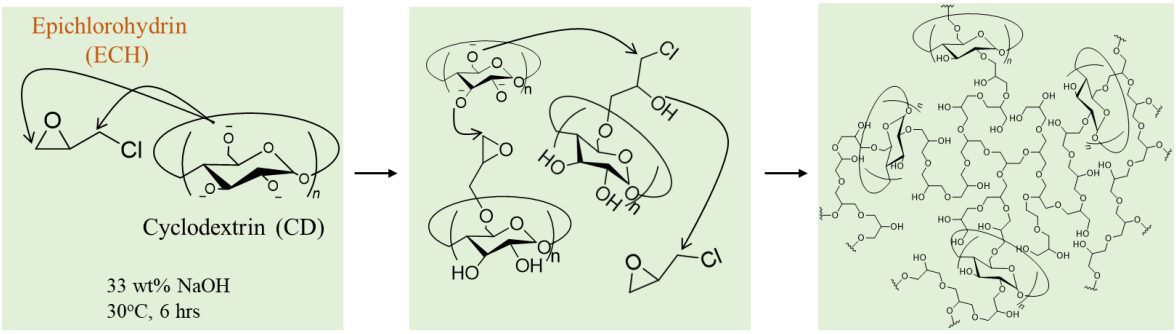

Figure 2-1. Synthesis scheme of cyclodextrin-based hyperbranched polymers (CDNPs) through polyaddition reactions with ECH.

We then present characterization results from light scattering technique to obtain properties of CDNPs such as weight-average molecular weight (M_w), hydrodynamic radius (R_h). In terms of weight percent of CD in one CDNP molecule ($wt\%_{CD}$) and number CD in one CDNP molecule (N_{CD}), we use acid sulfuric/phenol method for total carbohydrates. The most important aim of this chapter is to study how feeding weight ratio ECH/CD affects these nanoparticle properties.

II. 2 Experimental procedures

2. 1. Material

α-, β-, γCD, epichlorohydrin, and other solvents (≥99%) were purchased from Tokyo Chemical Industry Co., Tokyo Japan and used without further purification.

2. 2. Synthesis of CDNPs

All steps for synthesis was conducted as follows: 2 g of CD was added into 6.4 mL of 33 wt% NaOH solution and was stirred until CD was completely dissolved. Epichlorohydrin (2.4, 4.8, 7.2, 9.6, and 12.0 mL for βCD and 2.4, 4.8, and 7.2 mL for α- and γCD) was added to the reaction solution. The reaction solution was allowed to heat to 30°C and vigorously stirred for 6 hours, and then stopped by addition of acetone. The product precipitated, and then the unreacted ECH was decantated. The precipitant was dispersed in water and the solution was neutralized with 12N aqueous HCl. The polymer solution was purified by dialysis for 2 days using the membrane (of M_w cut-off 3500). During the dialysis, water-undissolved components were precipitated and we used the supernatant that was supposed to contain CDNPs. Three types of CD were used for the reaction with the various amount of epichlorohydrin in this study.

2. 3. Characterization techniques

SEC-MALS measurement was carried out for the CDNPs using Shodex column (SB802.5 and SB806) at 40°C with 10 mM aqueous NaCl as the eluent. We prepared the sample solution of 1 mg/mL in 10 mM aqueous NaCl. The solution was optically purified with PTFE membrane with 0.2 μm pore and injected it into the column. The output from the column was passed sequentially through a MALS detector (Wyatt Technology, Dawn HeleosII, wavelength: λ = 658 nm) and an RI detector (Wyatt Technology, 1.2-1.8 RIU, wavelength: λ = 488-690 nm). By use of MALS, the Rayleigh ratio (R_θ) was determined as a function of the scattering angle 2θ. We determined the specific refractive index increments ($\partial n/\partial c$) of the CDNPs in 10 mM aqueous NaCl with a differential refractometer (Otsuka Electronics DRM-1020, wavelength: λ = 633 nm). The sample concentration at the MALS detector was at most 1 mg/mL. It is dilute enough to neglect the concentration dependence of the scattering intensity. Therefore, R_θ can be given by:

$$\frac{Kc}{R_\theta} = \frac{1}{M_w}\left[1 + \frac{R_g^2}{3}(q)^2 + O(q^4)\right] + 2A_2c + O(c^2) \quad (3)$$

Here, K, M_w and R_g are the optical constant containing $\partial n/\partial c$, the weight-averaged molecular weight, and the z-averaged radius of gyration. The magnitude of the scattering vector q is determined by $q = (4\pi/\lambda)\sin\theta$. We used dynamic light scattering (DLS) to determine the hydrodynamic radius (R_h).

2. 4. Determination of carbohydrate concentration in CDNPs

CD weight percent in CDNPs was determined by the phenol sulfuric acid method [3]. Dried CDNP (0.025 g) was refluxed at 100°C for 8 hours in 0.5 M H_2SO_4 (15 mL) in order to break down the reacted CD to pentose. Then, solution was reacted with phenol 5% (w/w) and concentrated H_2SO_4. The final product turned into brown-orange color and the absorbance was detected by UV-Vis spectrophotometer (Jasco, V-630) at 488 nm and the absorbance was converted into the CD weight percent ($wt\%_{CD}$) by use of a calibration curve established glucose D(+) beforehand. Here, we confirmed that polymerized ECH did not show any absorbance after we treated them in the same manner. From the CD weight percent and M_w of CDNP, we calculated the number of CD in one CDNP particle (N_{CD}).

II. 3 Results and Discussion

3. 1. Characterization of CDNPs

Table 2-1 shows the sample code and the feeding weight ratio used in our experiment.

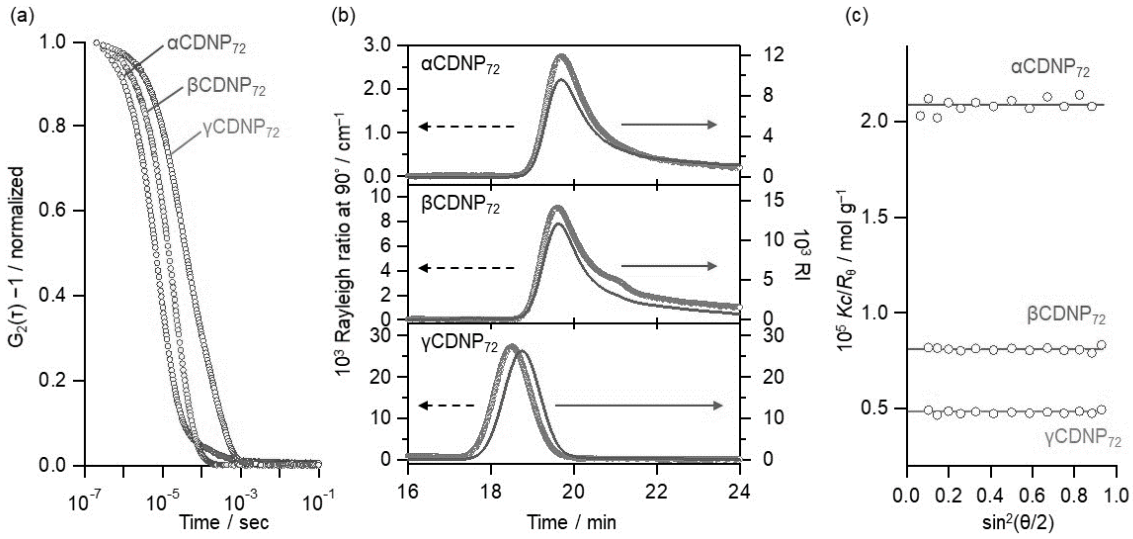

Figure 2-2. Examples of the particle characterizations for the series of $CDNP_{72}$. Autocorrelation function by use of DLS (a), SEC-MALS fractogram (b), and Zimm plot at the LS peak top of the fractogram (c).

The prefix and suffix of the sample codes in Table 2 indicate the type of CD and the amount of ECH, respectively. Figure 2-2 shows the autocorrelation function obtained by DLS, SEC-MALS fractogram, and the Zimm plot at the peak top for the series of $CDNP_{72}$ (the other results are shown in Figure S1 and S1). In the panel a, the autocorrelation functions

show unimodal feature in particle size and R_h at the peak top was listed in the Table 2-1. The panel b compares the chromatograms of the light scattering intensity at 90 degree and RI for the three samples. αCDNP$_{72}$ and βCDNP$_{72}$ showed a shoulder at the lower molecular weight, while γCDNP$_{72}$ did not. The panel c shows the angular dependence of R_θ for the same three samples. Extrapolating $q \to 0$, M_w was determined for all samples and listed in Table II-1. The angular dependence of the R_θ was negligibly small for all CDNPs, suggesting that the radius of gyration (R_g) may be 10 nm or less.

Table 2-1. Sample codes and properties of nanoparticles

Sample code	Feeding weight ratio	M_w [g/mol]	R_h [nm]	wt%$_{CD}$ [%]	N_{CD}
αCDNP$_{24}$		4.58 x10^4	1.82	77.0	38.5
βCDNP$_{24}$	1.42	7.95 x10^3	1.44	99.5	7.0
γCDNP$_{24}$		6.79 x10^3	1.53	92.6	4.8
αCDNP$_{48}$		4.87 x10^4	2.67	52.4	25.7
βCDNP$_{48}$	2.84	9.68 x10^4	4.10	55.6	47.4
γCDNP$_{48}$		8.53 x10^4	4.10	56.4	37.1
αCDNP$_{72}$		4.77 x10^4	2.65	51.9	25.5
βCDNP$_{72}$	4.26	1.44 x10^5	5.43	50.9	64.5
γCDNP$_{72}$		1.81 x10^5	5.25	52.0	72.7
βCDNP$_{96}$	5.68	2.80 x10^5	6.15	45.8	112.9
βCDNP$_{120}$	7.10	1.26 x10^5	4.62	46.3	51.4

M_w: Weight-average molecular weight
R_h: Hydrodynamic radius
wt%$_{CD}$: CD weight percent in one CDNP molecule
N_{CD}: Number of CD in one CDNP molecule

3. 2. The effect of Epichlorohydrin/Cyclodextrin on properties of CDNPs

Figure 2-3 plots M_w, N_{CD}, wt%$_{CD}$, and R_h against the feeding weight ratio of ECH to CD (ECH/CD). With an increase of ECH/CD, $wt\%_{CD}$ decreased from 77% to 50% for αCDNP and 99% to 50% for β- and γCDNP. These results indicate that the polymerized

ECHs were just connecting CDs at the feeding weight ratio of 1.42, whereas the polymerized ECHs formed a network between CDs at the other feeding ratio and the network portion increased with an increase of ECH/CD, then appeared to reach about 50%. This morphological difference is schematically illustrated in Figure 2-4. The other three parameters M_w, N_{CD}, and R_h increased and reached the maximum around ECH/CD=5.68 for βCDNP, while those for αCDNP were almost constant. This difference between αCDNP and the others may be owing to that the reaction of ECH went slowdown because the αCD cavity trapped ECH more tightly than the others. In fact, the binding constant between αCD and aliphatic ketones are higher than the others [4]. We presume that after ECH reacted with one of the hydroxyl group of αCD, the aliphatic moiety may go inside of the cavity accompanying the newly activated hydroxyl group and further chain reaction was reduced. When ECH/CD was 7.1, both M_w and R_h decreased. This is because that the reaction between ECH itself occurs too much, resulting in producing water-insoluble products. In fact, the yield at this condition was much lower than at other conditions.

We calculated the density $\rho = M_w/V_h$, where V_h is given by $4/3\,\pi R_h^3$, and the number CD per volume and weight by N_{CD}/V_h and N_{CD}/M_w, and plotted them against ECH/CD. αCDNP showed larger ρ and N_{CD}/V_h than the others, reflecting the higher $wt\%_{CD}$ than the others. For M_w, all three of $\alpha CDNP_{24}$, $\alpha CDNP_{48}$, $\alpha CDNP_{72}$ were appeared almost same, but ρ of $\alpha CDNP_{48}$ and $\alpha CDNP_{72}$ are lower than $\alpha CDNP_{24}$, indicating that $\alpha CDNP_{48}$ and $\alpha CDNP_{72}$ are sparser and less compressed than $\alpha CDNP_{24}$, because these two samples have more ECH network between αCDs. For β- and γCDNPs, the decreases in ρ and N_{CD}/V_h are less significant than that of αCDNP. For all samples, ρ and N_{CD}/V_h reached almost constant at ECH/CD>3, while N_{CD}/M_w were still decreasing in that region. When compared between βCDNP and γCDNP, N_{CD}/V_h were almost same, but N_{CD}/M_w of βCDNP was larger than that of γCDNP, reflecting the difference in the number of OH groups. Generally speaking, once ECH/CD>3, ρ and N_{CD}/V_h did not change so much, while the size was increased. This means that in the range of ECH/CD>3, there was no change in how CDs were distributed in the ECH network and how the ECH network were formed or packed, just the size was increasing. As a comparison experiment, when we polymerized ECH without CD, there was no water-soluble component because the obtained hyperbranched ECH polymers contains many ether bonds and a few hydroxyl groups and thus they are hydrophobic. This

fact suggests that the hydrophilic CDs tend to cover the surface of the particle, the inside consists of hyperbranched ECH and some CDs as illustrated in Figures 2-4a and 2-4b.

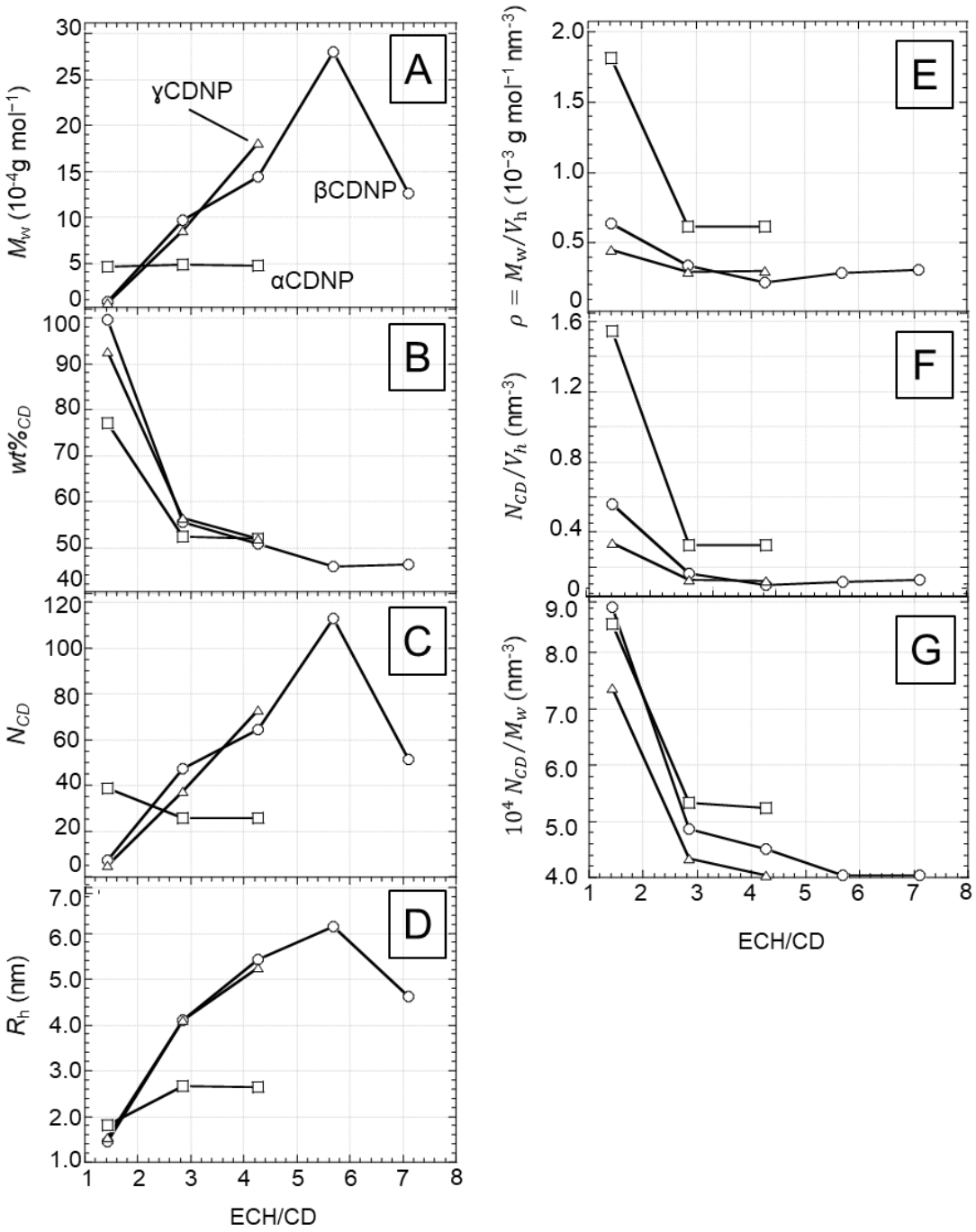

Figure 2-3. ECH/CD dependence of M_w (A), $wt\%_{CD}$ (B), N_{CD} (C), and R_h (D) for α (square), β (circle), and γ (triangle) CDNP. The density ρ and the number CD per volume and weight were plotted against ECH/CD in the panel of E, F, and G, respectively. Here the volume of the particle was calculated from V_h by $4/3\pi R_h^3$.

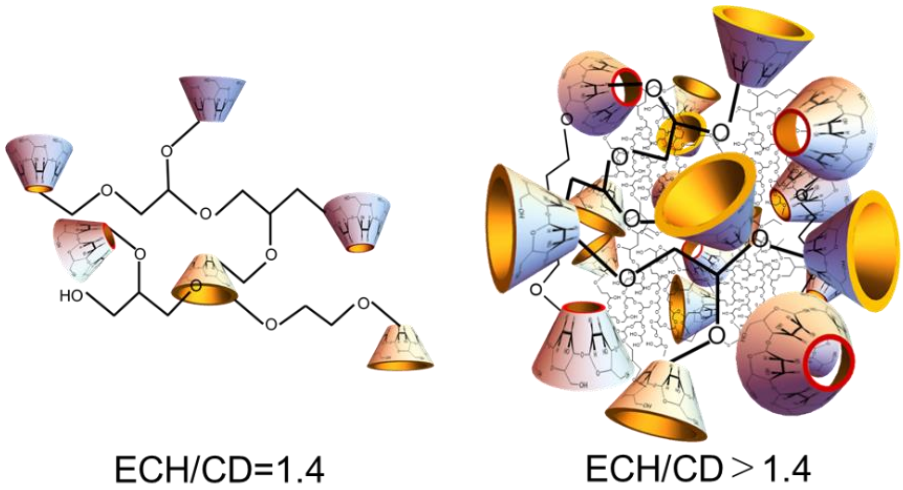

Figure 2-4. Schematic illustrations of CDNPs for different ECH/CDs. At ECH/CD=1.4, ECHs are just connecting CDs (truncated cone), while at ECH/CD>1.4 CDs are located at the surface of the particle to make it water-soluble, both the ECH network and some CDs occupy the inside.

Appendix: Characterization results of series of CDNPs

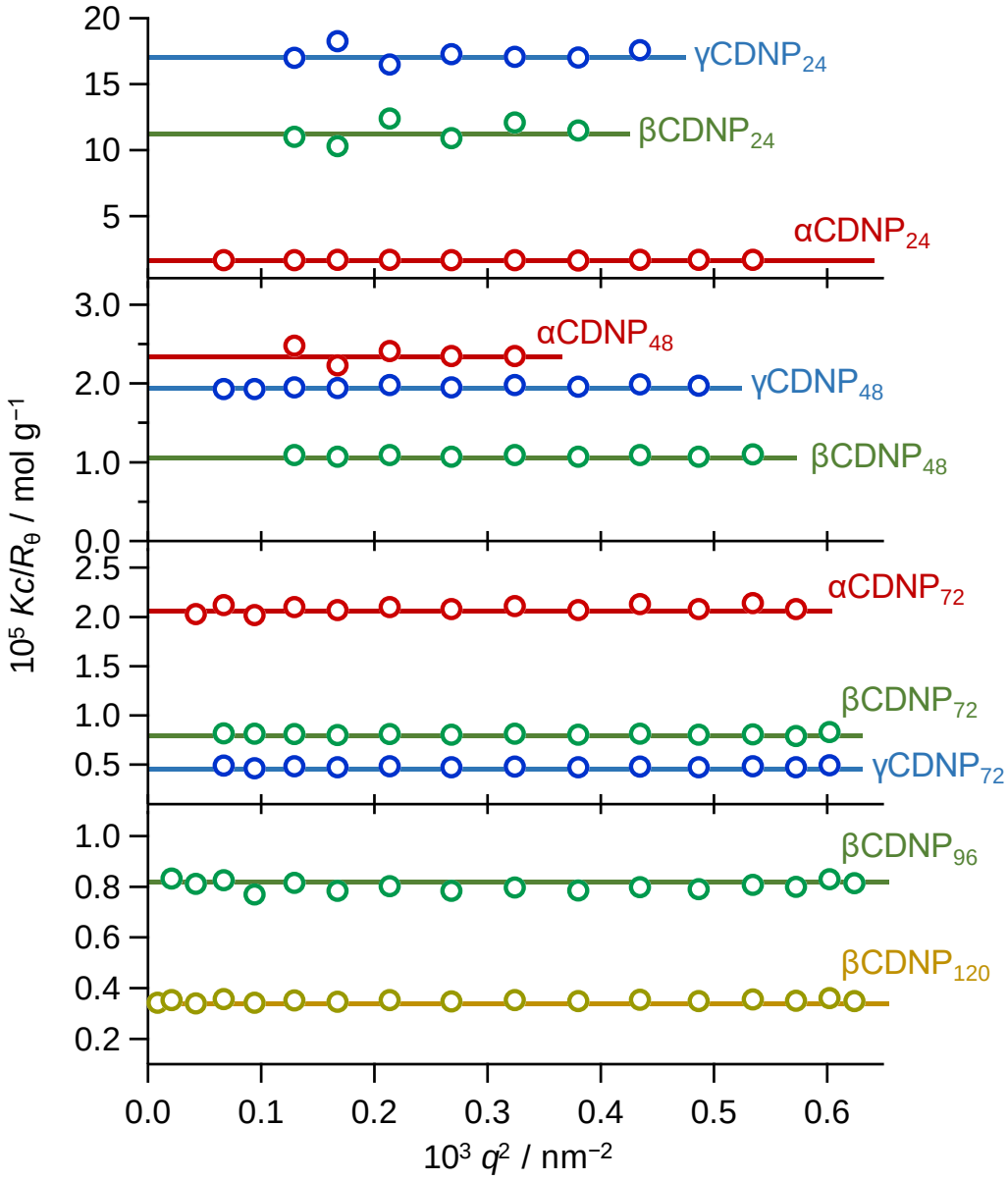

Figure 2-A1. Zimm plot at the LS peak top of the SEC fractogram for the series of the CDNPs.

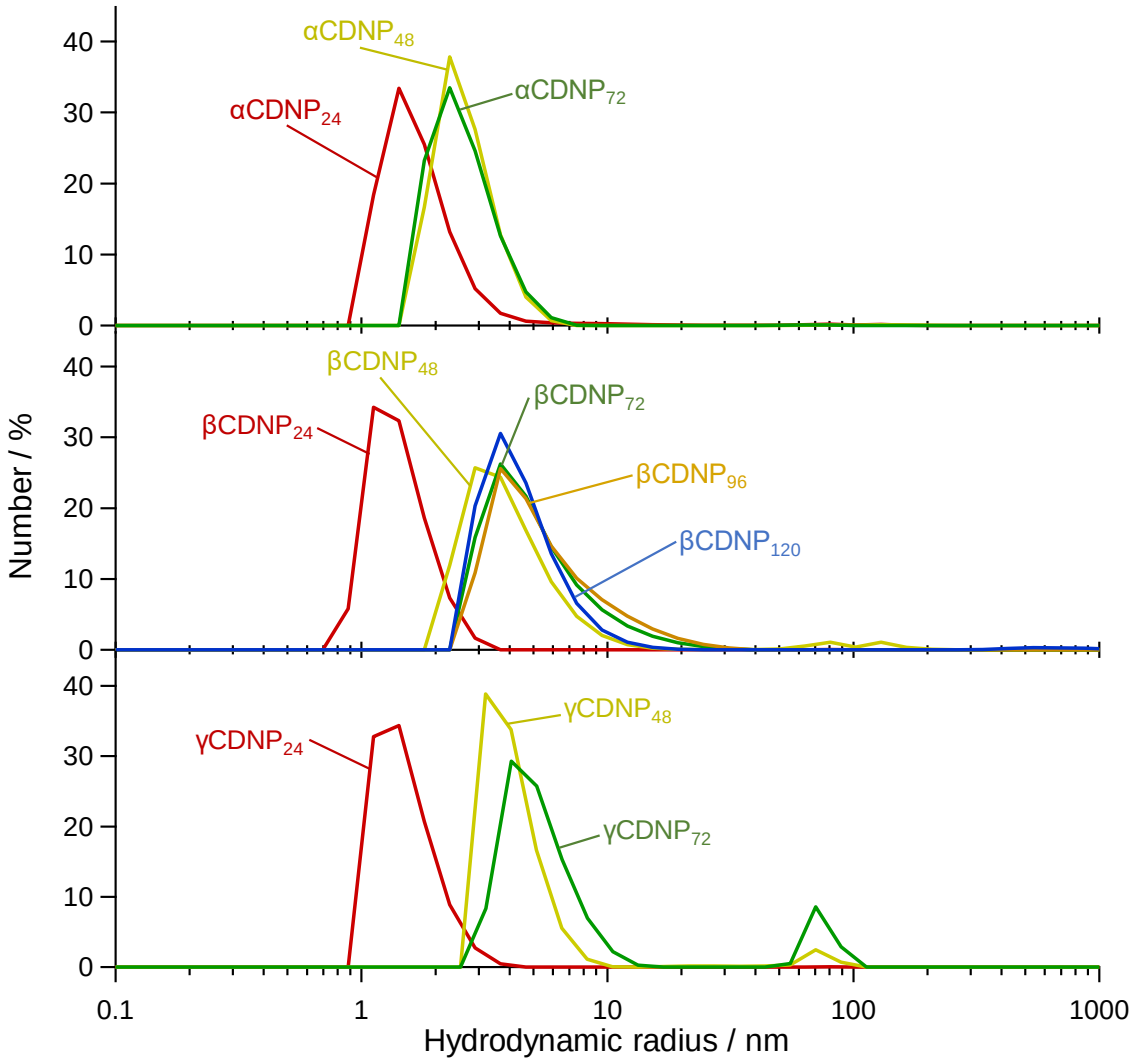

Figure 2-A2. Number size distribtuion of the CDNPs in water.

References

1 Renard E., Deratani A., Volet G. and Sebille B. Preparation and characterization of water soluble high molecular weight b-cyclodextrin-epichlorohydrin polymers. European Polymer Journal. 1997. 33: 49-57.

2 Salgın Sema, Salgın Uğur and Ayluçtarhan Mehmet. Synthesis of β-Cyclodextrin-Epichlorohydrin Nanospheres: Its Application for Removal of p-nitrophenol. American Chemical Science Journal. 2016; 16: 1-10. 10.9734/acsj/2016/29198.

3 Heydari Abolfazl, Hassani Yeganeh, Sheibani Hassan and Pardakhti Abbas. Water-Soluble β-cyclodextrin Polymers as Drug Carriers to Improve Solubility, Thermal Stability and Controlled Release of Nifedipine. Pharmaceutical Chemistry Journal. 2017; 51: 375-83. 10.1007/s11094-017-1617-0.

4 Oswald S. Tee, Alexei A. Fedortchenko, Paul G. Loncke and Timothy A. Gadosy. Binding of aliphatic ketones to cyclodextrins in quaeous solution. Journal of the Chemical Society, Perkin Transactions. 1996. 2: 1243-49.

Chapter III. The ability of encapsulating Alpha mangostin in aqueous solution

III. 1 Introduction

As mentioned in Chapter I, the structure of CDs enables CDs to capture hydrophobic compounds inside them; the resultant complex can still maintain water-solubility, which is very advantageous for delivering hydrophobic compounds to biological systems [1]. Thus, in the preceding chapter, we examine whether CDNPs have the ability of encapsulating MGS or not. Chapter III presents loading ratio of MGS incorporated into native CDs and CDNPs.

Additionally, the inclusion of hydrophobic compounds into CDs involves the typical host and guest supermolecular interaction without covalent bonds [1]. Determining the binding constant for such a host-guest interaction is one of the central issues in supramolecular chemistry. Although techniques such as nuclear magnetic resonance spectroscopy and isothermal titration calorimetry could be useful for this purpose, they may not work or be inappropriate for some compounds when the guest molecule has very poor water-solubility [2]. We use an alternative method which has been used for CDs to evaluate the complexation efficiency between CD and guest molecules [3-6]. The complexation efficiency value can be related the binding constant. The interaction between CD and MGS is presented after loading ratio results.

One of the most advantages of nanoparticles is to control drug release [7]. To end this chapter, drug release profile of MGS in aqueous solution is performed. The release properties will be a prediction about cytotoxic behavior of CDNP/MGS complexes *in vitro* and *in vivo* experiment in next chapter.

III. 2 Experimental procedure

2. 1. Preparation of CDNP/MGS complex and determination of loading ratio

An MGS in DMSO solution (50 µL, 10, 50, and 100 mM) was added to the CDNP solution (450 µL, 10 mg/mL). The mixture was kept at room temperature for 2h. After centrifugation (12,000 rpm for 5 min), the upper solution was collected and purified by dialysis (cut-off Mw = 3500 g/mol). The solution was finally filtered. The absorbance of MGS at 323 nm was detected by a UV–Vis spectrophotometer, and the loading ratio of MGS into the CDNPs was determined.

2. 2. Field Flow Fractionation coupled with UV and RI (FFF)

To confirm the inclusion of MGS by CDNPs, AF4-MALS measurements were used in this study. They were performed using an Eclipse 3+ separation system (Wyatt Technology Europe GmbH, Dernbach, Germany) at a channel-flow rate of 3 mL/min and a gradient cross-flow. The AF4 system is equipped with a Dawn Heleos II MALS detector (Wyatt Technology) and an Optilab rEX DSP differential refractive index detector with the wavelength of 658 nm (Wyatt Technology).

2. 3. Solubility study

Theorical background

MGS and CDs are assumed to form a 1:1 complex stoichiometrically:

$$\mathrm{MGS} + \mathrm{CD} \overset{K_{1:1}}{\leftrightarrow} \mathrm{MGS/CD}$$
$$K_{1:1} = \frac{[\mathrm{MGS/CD}]}{[\mathrm{MGS}][\mathrm{CD}]} \tag{1}$$

Here, $K_{1:1}$ is the binding constant. With a given total concentration of cyclodextrin in aqueous solution $[\mathrm{CD}]_t$ ($\equiv [\mathrm{MGS/CD}] + [\mathrm{CD}]$) and the intrinsic solubility of MGS: S_0 (i.e., the solubility in aqueous medium when no CD is present), the total MGS concentration (S_{total}) in aqueous solutions is given by:

$$S_{\mathrm{total}} = S_0 + \frac{K_{1:1}\, S_0}{1 + K_{1:1}\, S_0}[\mathrm{CD}]_t \equiv S_0 + \chi[\mathrm{CD}]_t \tag{2}$$

Eq. 2 shows that, when S_{total} is plotted against $[\mathrm{CD}]_t$, the plot should constitute a straight line with slope χ and intercept S_0. Therefore, from the slope and the intercept of this plot, we can determine $K_{1:1}$ from $K_{1:1} = \chi/[S_0(1-\chi)]$. However, MGS shows a very low saturated solution concentration at ambient temperature (c.a., 4.95×10^{-10} M) [3,8] and thus S_0 determined from the intercept may have large error. Alternatively, we can determine the product of $S_0K_{1:1}$ only from the slope. Hereinafter, we define this value as the complexation efficiency (CE). The above method was originally presented by Higuchi and Connor [3] and since then has been used in a several CD related systems [3-6].

Experimental methods

To determine the complexation efficiency, 2.5 µL of MGS (10 mM/L in DMSO) was added to a α-, β-, or γCD aqueous solution (497.5 µL) whose concentration ranged from 1.0 to 20 mM. In CDNP system, 5 µL of MGS (30 mM/L in DMSO) was added to a α-, β-, or γCDNP aqueous solution (495 µL) whose concentration ranged from 6.25×10^{-4} to 0.2 mM. These mixtures were placed at room temperature for 2h and then centrifuged twice at 12,000 rpm for 5 min to remove the precipitated MGS. The supernatants were collected and measured by UV–Vis spectrophotometry to determine the total concentration (S_{total}) of solubilized MGS owing to the presence of CD.

2. 4. Drug release profile

From this section to the end of thesis, we chose CDNPs at weight ratio ECH/CD of 4.26, where 7.2 mL of epichlorohydrin (ECH) was reacted with 2.0 g of CD. As presented in the previous Chapter II, we found that this reaction composition gives the maximum particle size and the highest CD composition without creating a large amount of insoluble components. Hereinafter, αCDNP, βCDNP, and γCDNP were used in place of $\alpha CDNP_{72}$, $\beta CDNP_{72}$, and $\gamma CDNP_{72}$.

MGS-incorporating αCDNP, βCDNP and γCDNP in 150 mM NaCl solution were placed in a membrane dialysis bag and then the bag was transferred into a flask containing 60 mL of the same buffer solution and kept at 37°C. The bulk solution was continuously stirred with a magnetic stirrer. Solution samples (20 µL) were withdrawn at selected intervals (0, 1, 2, 4, 6, 18, 24, and 48h) and replaced with equal volumes of fresh buffer. The quantity of released MGS was determined by UV-Vis spectrophotometry at 323 nm.

III. 3 Results and Discussion

3. 1. Loading ratio of MGS

Figure 3-1a shows FFF fractograms for $\beta CDNP_{48}$ before and after adding MGS. $\beta CDNP_{48}$ was detected at approximately 16 min by RI, but this peak had no UV absorbance at 323 nm, whereas for $\beta CDNP_{48}$/MGS, the UV signal appeared at the same peak position as RI, indicating that $\beta CDNP_{48}$ successfully encapsulated MGS. When we tried to determine the loading ratio of MGS to CDNPs from the ratio of the UV and RI peak areas, it was always lower than expected, and there was no reproducibility. We suppose that this is due to the adsorption of MGS onto the cellulose acetate membrane in the FFF channel. This is called the “focusing problem” in FFF. Before starting the fractionation, the injected sample was

placed at a certain position on the cannel by use of a combination of backward and forward flows. This process is called “focusing”, and backward and forward flows are tuned to pin the sample on a membrane filter; therefore, the solutes are strongly pushed against the surface of the membrane. When the solutes contain some hydrophobic compounds, they may be transferred and absorbed by the membrane filter. Instead of using FFF, the loading ratio for each CDNP was determined by UV–Vis measurements, assuming no water-solubilized MGS in the solution.

Figure 3-1b plots the loading ratio of MGS against the feeding ratio, compared with those of three CDNP, i.e., α-, β-, γCDNP$_{72}$, and native CDs. Surprisingly, all of the CDNP/MGS complexes showed a much larger loading ratio than CDs themselves. The loading ratio follows the order of β > γ > α for both CD and CDNP, which is consistent with the CE values. As expected, βCDNPs always have the best loading ratios (Table 3-1). The maximum loading ratios (Max.L_{MGS}) of α-, β-, and γCD are 0.060, 0.60, and 0.22%, respectively; in other words, the loading ratios of native CDs are slightly less than 1%. However, those of CDNPs significantly increased. For example, βCDNP$_{72}$/MGS reached 10.7%, ~17 times as high as βCD/MGS.

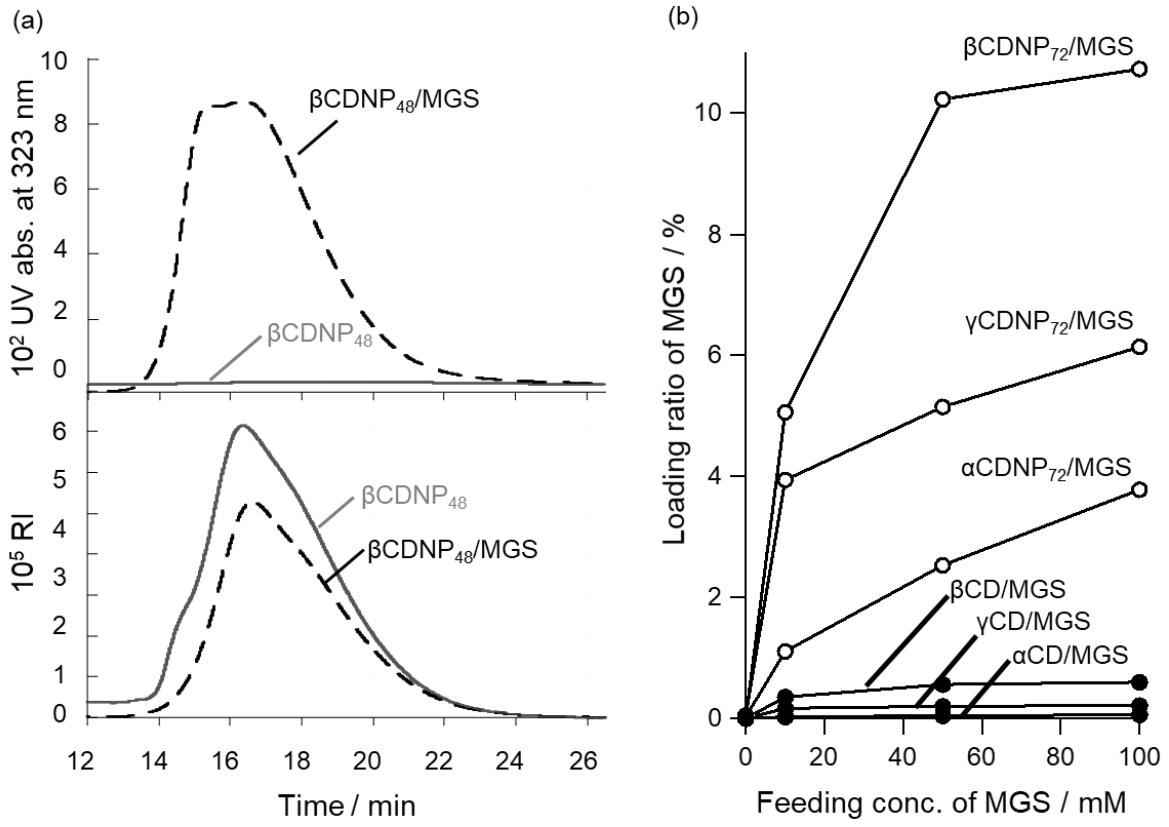

Figure 3-1. (a) AF4-UV-RI fractogram of $\beta CDNP_{48}$ and $\beta CDNP_{48}$/MGS in 10 mM aqueous NaCl. (b) The dependence of feeding concentration of MGS on the loading ratio of it for CDNPs and native CDs.

Table 3-1. Maximum loading ratio (Max.L_{MGS}) and molar ratio of CD to MGS in CDNP/MGS complexes

Sample code	Max.L_{MGS} [% wt]	[CD]/[MGS]
$\alpha CDNP_{24}$	2.12	17.5
$\beta CDNP_{24}$	6.23	5.8
$\gamma CDNP_{24}$	5.13	6.5
$\alpha CDNP_{48}$	3.04	8.0
$\beta CDNP_{48}$	8.38	2.6
$\gamma CDNP_{48}$	7.29	2.7
$\alpha CDNP_{72}$	3.78	6.4
$\beta CDNP_{72}$	10.73	1.9
$\gamma CDNP_{72}$	6.14	3.0
$\beta CDNP_{96}$	13.67	1.3
$\beta CDNP_{120}$	15.32	1.1

We already knew the weight percent of CD in CDNP. From this, we calculated how many CDs are involved in the complexation in terms of [CD]/[MGS] and plotted this value against ECH/CD in Figure 3-2. [CD]/[MGS] in the CDNP systems approaches 1 with increasing ECH volume. There may be two possible explanations for this enhanced uptake of MGS by CDNP. One is that the chemical modification of CD with ECH somehow enhanced the binding between MGS and CD. Such an enhancement is sometimes observed, as shown by previous studies [5,9]. For example, it has been observed that the hydroxypropylation of OH groups at the O-2 position of CD results in a more spread out CD configuration. In this case, the binding ability is enhanced. However, the substitution of OH groups at the O-6 position reduces the water density inside the CD cavity [10]. This theory

can explain the result that [CD]/[MGS] appeared to asymptotically converge to [CD]/[MGS] = 1 at higher ECH/CD values. However, the cavity size of αCD seems too small to fit MGS, and it is unlikely that even chemical modification will improve the binding between MGS and αCD. Another explanation is that the hyperbranched ECH network inside the polymer molecule is also so hydrophobic that it might encapsulate MGS as well as the cavity of CDs. Similar behavior has been observed in other cases. Alsbaiee et al. prepared βCD-containing polymers by use of a reaction similar to that of the present study between βCD and tetrafluoroterephthalonitrile [11]. The resultant polymers had a high surface area that could absorb many hydrophobic compounds, and their performance was as good as that of active carbons. Such an increased number of binding sites due to polymerization is called the "expanded pocket". We can presume that similar phenomena occurred in our system. Figure 3-2b illustrates such additional binding sites created by the ECH network.

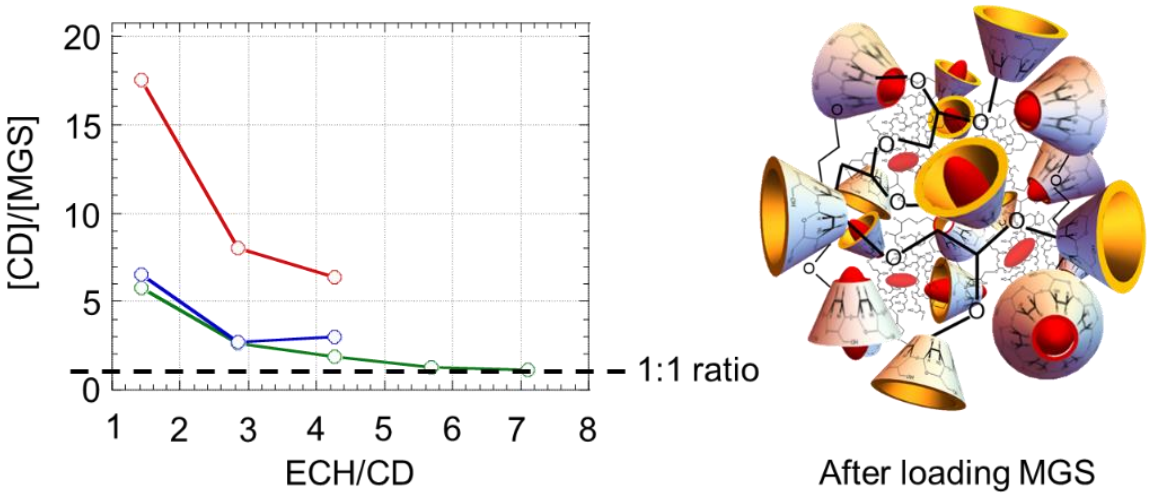

Figure 3-2. (a) Relationship between [CD]/[MGS] and feeding ratio ECH/CD. (b) After loading MGS **(**red ellipse), CD and the hydrophilic ECH may capture the drugs.

3. 2. Interaction between CD and MGS

In section 3.1, CDNPs performed the ability of encapsulating MGS with great loading ratio in aqueous solution. We assumed that the interaction between CDs and MGS was enhanced by polymerization. We considered a simple model of reaction, where one MGS molecule form with one CD molecule in order to evaluate roughly binding constant as described in "Experimental procedure". Figure 3-3 plots S_{total} against $[\mathrm{CD}]_{\mathrm{t}}$ for three CDs

and three CDNPs: αCDNP$_{72}$, βCDNP$_{72}$, and γCDNP$_{72}$, constructed from S_{total} (determined from the UV–Vis spectra for each complex; see Figure 3-A1 to A8) and [CD]. The data points for each CD and each CDNP can be fitted by a straight line passing through the origin, meaning that the interaction between CD and MGS follows a 1:1 ratio (A_L type), but S_0 was too small to be determined. From the slopes, CE was determined to be 4.0×10^{-4}, 1.1×10^{-2}, and 6.5×10^{-3} for αCD, βCD, and γCD, respectively. These values are summarized in Table 3-2 with those of other compounds. αCD can hardly solubilize MGS, while βCD and γCD relatively solubilize it, and βCD showed a larger CE than γCD, demonstrating that βCD is the most suitable. Our results confirm previous studies. Compared with the values for other compounds, the CE for MGS/CD is not significantly large but is similar to that of cyclosporine A.

In CDNPs system, it is clear that βCDNP showed larger CE than the other two samples. In our previous section, we determined the maximum loading capacity and found the order of βCDNP > γCDNP > αCDNP in terms of the affinity for MGS. The result for CE is consistent with the previous ones. Upon carefully examining βCDNP$_{72}$, the data points appeared to exhibit slight convexity upward, instead of being fitted by a straight line. This suggests that 1:1 binding may not be the only mode, as discussed below. Figure 3-3 also shows a significant difference between native CDs and CDNPs. The most important conclusion from Figure 3-3 is that all CE values are dramatically increased (about 100 times) by ECH polymerization, compared with CDs themselves.

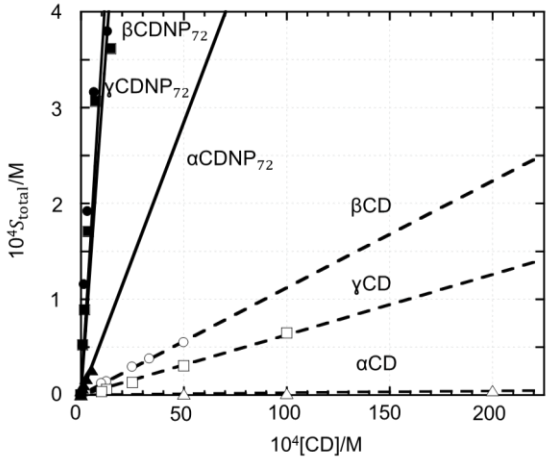

Figure 3-3. S_{total} and $[CD]_t$ plot of MGS-CDNP$_{72}$ with curve fit (solid line) and MGS-native CDs with curve fit (dotted line).

Table 3-2. The complexation efficacy of some drugs against CDs and their derivatives

Drug/Compound	Cyclodextrin	CE	Reference
MGS	αCD	4.0×10^{-4}	This work
MGS	βCD	1.1×10^{-2}	This work
MGS	γCD	6.5×10^{-3}	This work
MGS	$\alpha CDNP_{72}$	0.06	This work
MGS	$\gamma CDNP_{72}$	0.77	This work
MGS	$\beta CDNP_{24}$	0.37	This work
MGS	$\beta CDNP_{48}$	1.03	This work
MGS	$\beta CDNP_{72}$	1.08	This work
MGS	$\beta CDNP_{96}$	1.77	This work
MGS	$\beta CDNP_{120}$	-	This work
Acetazolamide	HPαCD	1.5×10^{-2}	[9]
Cyclosporine A	αCD	1.1×10^{-2}	ibd
Diethylstilbestrol	HPβCD	2.8	ibd
Finasteride	RMβCD	0.7	ibd
Progesterone	HPγCD	0.2	ibd

2-hydroxypropyl-α-cyclodextrin (HPαCD); 2-hydroxypropyl-β-cyclodextrin (HPβCD);

randomly methylated β-cyclodextrin (RMβCD); 2-hydroxypropyl-γ-cyclodextrin (HPγCD);

Figure 3-4a compares different ECH compositions for βCDNP series, showing that the slope increased with an increase of ECH. Figure 3-4b plots the ECH dependence of CE. We have already confirmed that there was no binding between polymerized ECH and MGS

without CD. This was despite CE increasing with increasing ECH, almost linearly. This is an interesting phenomenon.

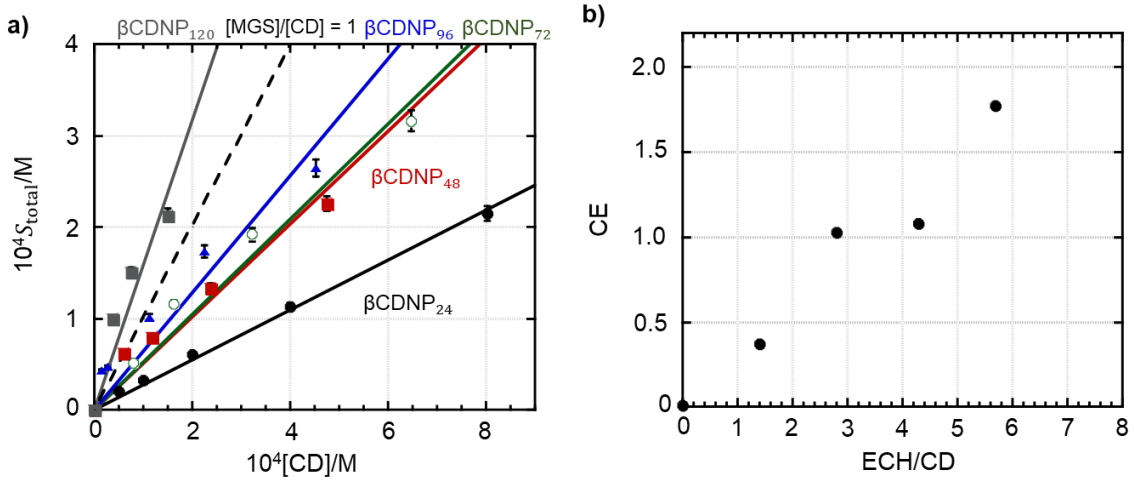

Figure 3-4. (a) The ECH feeding ratio dependence of the solubility in βCDNP system. (b) The obtained CE was plotted against the feeding weight ratio ECH/CD. The dotted line in (a) is the ideal binding in the case of $K_{1:1} = \infty$.

In the extreme case that $K_{1:1} = \infty$, meaning that all of the added MGS and CD are interacting, the S_{total} vs. $[\text{CD}]_t$ plot should follow $S_{\text{total}} = [\text{CD}]_t$, which is indicated by the dotted line in Figure III-4a. βCDNP$_{96}$ appeared to follow the dotted line in the region of with low $[\text{CD}]_t$ and surprisingly βCDNP$_{120}$ went beyond this limit. These facts indicate that 1:1 binding is not the only mode to capture MGS for βCDNP$_{120}$ and βCDNP$_{96}$, modes of binding at ratio of 2:1 or more of MGS to CD may be involved. This may be the reason for the observed upward convexity from a straight line. At present, we do not have any clear explanation for this, but we can speculate the following: ECH polymerization converts OH groups of CD to ether groups and thus ECH polymerization may increase the hydrophobicity of the upper and lower rims of CD. The OH groups on the rims may interfere with hydrophobic interaction between MGS and the inside of CD. In other words, it may be possible for hydrophobic compounds like MGS to more easily enter the cavity of CD due to the elimination of some OH groups of CD during the ECH polymerization. To support this speculation, the interaction between MGS and modified OH groups in βCD (2-hydroxylpropyl-βCD) was investigated (Figure 3-A9). It is found that CE of 2-hydropropyl-βCD/MGS increased 7 times in comparison with βCD/MGS, suggesting the modification of the OH group would affect and improve the interaction between βCD and MGS. However,

this increment was still small compared to that in polymer system, indicating other factors might be involved in the large increment of the binding constant.

With a given literature value for S_0 of MGS (4.95×10^{-10} M, PubChem) [12], $K_{1:1}$ is roughly estimated as shown in Table 3-3, compared with other systems including a typical ligand-receptor interaction in biological systems. The $K_{1:1}$ values for native CD and MGS appear to be equal to or slightly greater than those for typical CD complex systems such as adamantane-βCD [13] and cholesterol-βCD [14]. As reported, the interaction of drug vs. plasma protein is closely related to the pharmacokinetics and pharmacodynamics or distribution of the drug. When drugs exhibit strong binding to plasma proteins, they may not interact with their target, and may be metabolized or excreted. The binding constants of MGS to human serum albumin (HSA) and human transferrin in plasma were determined to be 6.48×10^5, and 1.46×10^5, respectively, according to Guo et al [15]. Compared with these, the interaction between MGS and CD has a higher binding constant; thus, it might not dissociate in blood circulation and might reduce these weaknesses of plasma protein binding. For the present systems, the binding constant reaches 10^9 (M^{-1}), being at the same level as antigen-antibody interaction.

Table 3-3. The comparison of binding constant between CDNP-MGS and some biological interaction

Interaction	K (M^{-1})	Reference
MGS-αCDNP$_{72}$	$1.22\times10^{8} \pm 4.26\times10^{6}$	This work
MGS -γCDNP$_{72}$	$1.56\times10^{9} \pm 5.46\times10^{7}$	This work
MGS-βCDNP$_{24}$	$7.59\times10^{8} \pm 2.66\times10^{7}$	This work
MGS-βCDNP$_{48}$	$2.08\times10^{9} \pm 7.29\times10^{7}$	This work
MGS-βCDNP$_{72}$	$2.19\times10^{9} \pm 7.66\times10^{7}$	This work
MGS-βCDNP$_{96}$	$3.59\times10^{9} \pm 1.26\times10^{8}$	This work
1-carboxyadamantane - βCD	2.8×10^{4}	Schibilla et al [13]
Cholesterol - βCD	1.7×10^{4}	Frijlink et al [14]
MGS - HSA	7.86×10^{5} (310K)	Guo et al [15]
MGS - TRF	1.15×10^{5} (310K)	Guo et al [15]
Monoclonal IgG_1 MA2.1 antibodies - HLA 2	1.2×10^{9}	Ways et al [16]
Antiviral antibodies - antigen (influenza viruses)	10^{6}-10^{10}	Frankel et al [17]
IgG - hapten (4-hydroxy-3-nitrophenyl)acetic acid	10^{9}	Tobita et al [18]

HSA: human serum albumin; TRF: transferrin; HLA: human transplantation antigen

3. 3. Drug release profile of MGS in aqueous solution

Among series of cyclodextrin-based hyperbranched nanoparticles, we chose a representative sample including αCDNP$_{72}$, βCDNP$_{72}$, and γCDNP$_{72}$ (hereinafter, αCDNP, βCDNP, and γCDNP, respectively) in this experiment. Figure 3-5 shows a semilogarithmic plot of the concentration of MGS retained by CDNP in 150 mM NaCl at 37℃ against time, comparing αCDNP, βCDNP, and γCDNP. All samples showed two-step decay: the initial

rapid release and the second slow release. Therefore, we fitted the data by using the following equation consisting of two exponential decays:

$$C(t) = C_1 \exp\left(-\frac{t}{\tau_1}\right) + C_2 \exp\left(-\frac{t}{\tau_2}\right) \quad (3)$$

Here, τ_1 and τ_2 are the times to characterize each decay mode or the lifetimes. C_1 and C_2 are the weight fractions of each mode. The solid lines in the figure are the best fitted curves calculated from Eq. 3 and the obtained parameters are summarized in Table 3-4. The obtained C_2 values were in the range of 75%–82 %, indicating that most of MGS was released in this slow mode. τ_1 is similar in βCDNP/MGS and γCDNP/MGS, but smaller in αCDNP/MGS than the others. For τ_2, in contrast, βCDNP/MGS shows a value three times longer than the others.

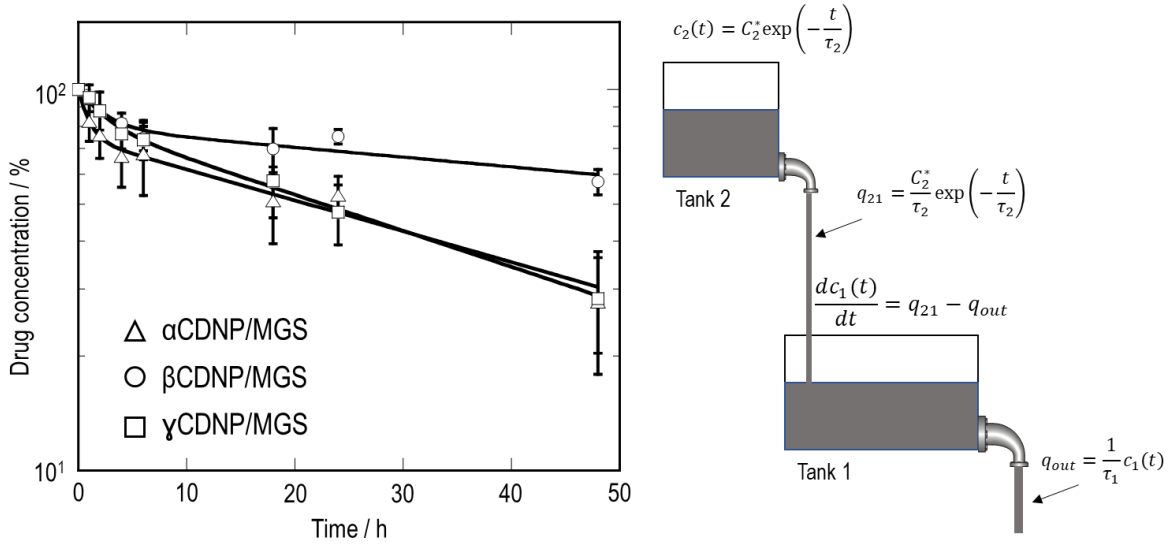

Figure 3-5. The profiles of the release of MGS from αCDNP, βCDNP and γCDNP in 150 mM NaCl at 37°C, where the solid curves were calculated using Eq. 1 (left) and the two-tank model to mathematically describe their release behaviors (right).

Table 3-4. Fitting parameters of release profile

Sample code	C_1 (%)	$\boldsymbol{\tau_1}$ (hr)	C_2 (%)	$\boldsymbol{\tau_2}$ (hr)
αCDNP/MGS	25.7	1.0	74.3	53.6
βCDNP/MGS	22.0	2.4	79.2	170
γCDNP/MGS	19.5	2.5	81.8	45.9

The concentration decay that follows a bi-exponential expression such as Eq. 1 is obtained from the model in which two tanks are connected in series, as shown in Figure 3-5. Here, Tank 2 has the initial value of C_2^* and it decays with the characteristic time of τ_2. The inflow from Tank 2 is denoted by q_{21} and the relationship of $q_{21} = (C_2^*/\tau_2)\exp(-t/\tau_2)$ holds. The outflow from Tank 1 is q_{out} and $q_{out} = c_1(t)/\tau_1$, where $c_1(t)$ is the value of Tank 1. The release of MGS from CDNP to NaCl solution corresponds to q_{out} and the drug concentration measured in Figure 3 is given by $c_1(t) + c_2(t)$. Here, the fluxes (i.e, q_{out} and q_{21}) are assumed to follow the Fick's law of diffusion. Considering the mass balance in Tank 1, we can obtain the following differential equation:

$$\frac{dc_1(t)}{dt} = \frac{C_2^*}{\tau_2}\exp\left(-\frac{t}{\tau_2}\right) - \frac{1}{\tau_1}c_1(t) \tag{2}$$

Assuming Tank 1 has the initial value of C_1^*, this equation gives the following relation:

$$c_1(t) + c_2(t) = C_2^*\frac{\tau_2}{\tau_2 - \tau_1}\exp\left(-\frac{t}{\tau_2}\right) + \left\{C_2^*\left(\frac{-\tau_1}{\tau_2 - \tau_1}\right) + C_1^*\right\}\exp\left(-\frac{t}{\tau_1}\right) \tag{3}$$

In the case of $\tau_2 \gg \tau_1$, Eq. 3 becomes identical to Eq. 1 and $C_1^* = C_1$ and $C_2^* = C_2$. This means that Tank 2 corresponds to the slow release in the experiment. The important conclusion derived from this model is that there is no path to release MGS directly from Tank 2 to the outside, and MGS always has to go through Tank 1 before release.

Another potential model, where we assume that the modified and unmodified CDs individually present in solutions, can provide the two exponential decays. In the model, the modified and unmodified CDs correspond to the CD located inside and surface of CDNPs, respectively. However, when MGS release from internal CDNP, it must go through the surface CD, meaning that the more reasonable model is the two-tank model described in Figure 3-5.

Comparing Table 3-4 and the tank model, 70-80% of MGS is held in Tank 2 in the initial state and the transfer from Tank 2 to Tank 1 determines the second slow release. What molecular mechanism corresponds to each tank and the fluxes from the tanks? We can assume that there are two possible mechanisms, as illustrated in Figure 3-6. First, before release into water, MGS has to escape from CDs and move to the hydrophobic domain, which may be made from polymerized epichlorohydrin (Model 1). Second, there are two types of CD: one exhibits strong MGS binding and the other less strong binding; before release, MGS has to move from the strong one to the less strong one. Our previous study suggested that the polymerized epichlorohydrin has no ability to absorb MGS; therefore, model 2 is more likely. CDs are water-soluble and polymerized epichlorohydrin without CDs is insoluble in water. Therefore, the good water solubility of CDNPs indicates that the surface of CDNPs is coated by CDs. Table 2-1 shows that 50 wt% of CDNP is composed of CDs. Such high content cannot be achieved only by the level of CDs on the surface. It is thus reasonable to assume that many CDs are contained inside the CDNPs. If there are some CDs inside the CDNPs, their OH groups have been converted to ethers during the polymerization and these internal CDs are more hydrophobic than those on the surface. Therefore, we can assume that the internal CDs show more affinity than the surface ones. In this context, we can propose the following model for the release profiles (also illustrated as Model 3 in Figure 3-6). CDNPs consist of two types of CD: internal CDs, which strongly bind to MGS and surface CDs which show less strong binding to MGS The initial rapid release corresponds to the release from the surface CDs. The internal CDs contain 70% MGS, and these MGSs are slowly transferred from the interior to the surface. This process corresponds to the mass transfer from Tank2 to Tank1 described in Figure 3-5 and no direct release from the interior to water. After MGS is captured by the surface CDs, it is rapidly released into water.

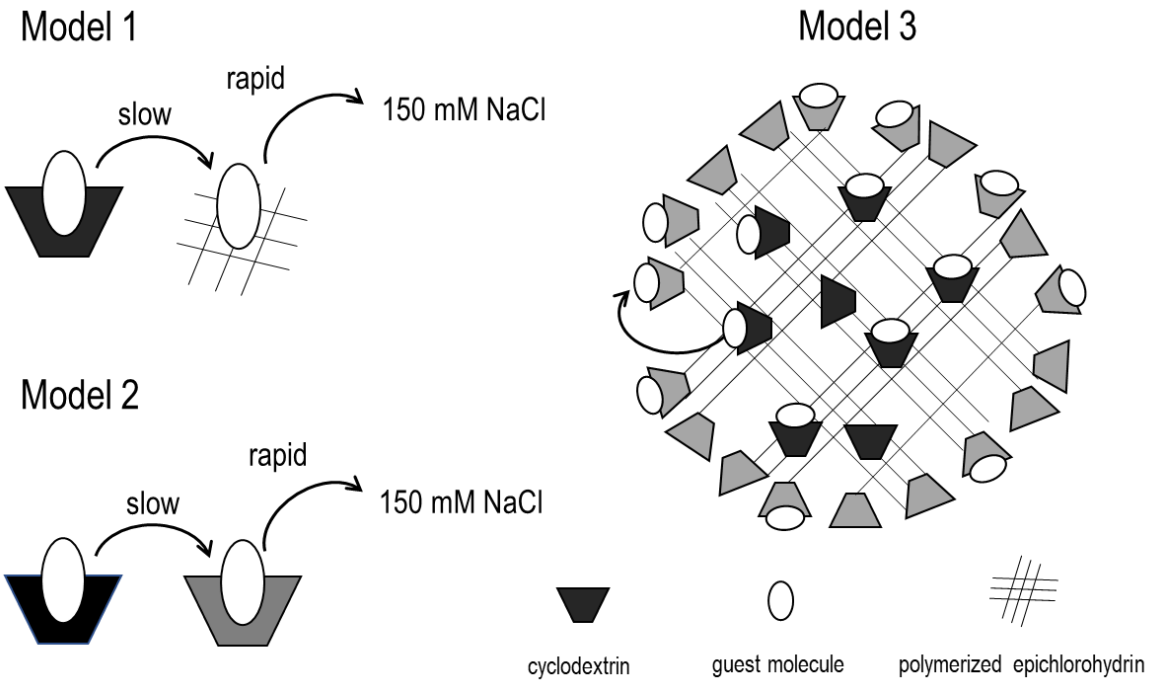

Figure 3-6. Two possible basic models to explain the two-step release and the molecular model for MGS release from CDNP.

The binding constant (*K*) data in Table 3-3 indicates that βCDNP and γCDNP showed similar values of *K*. Here *K* is given by $K = [\mathrm{CD/MGS}]/[\mathrm{CD}][\mathrm{MGS}]$, assuming the following 1:1 reaction:

$$[\mathrm{MGS}]+[\mathrm{CD}] \underset{k_a}{\overset{k_d}{\leftrightharpoons}} [\mathrm{CD/MGS}] \tag{4}$$

In this reaction, k_d and k_a are the dissociation and association rate constants and $K = k_a/k_d$ holds. From the release experiment and its mathematical analysis, it is easily deduced that τ_2 is related to $[\mathrm{CD/MGS}]$ through $d[\mathrm{MGS}]/dt = (1/\tau_2)[\mathrm{CD/MGS}]$. This means that $k_d = 1/\tau_2$. The binding constant can be defined in the equilibrium state, while the dissociation and association rate constants show the kinetical properties. The facts of $K_\beta \sim K_\gamma$ and $\tau_{2\beta} > \tau_{2\gamma}$ mean that the relationship of $k_{d\gamma} > k_{d\beta}$ and $k_{a\gamma} > k_{a\beta}$ hold in Eq. 4, where the subscripts indicate the types of CD. In other words, the concentration of released MGS is almost the same at the equilibrium for both βCDNP/MGS and γCDNP/MGS, but

γCDNP/MGS more rapidly releases MGS than βCDNP/MGS, with a difference of about four times ($k_{d\gamma}/k_{d\beta} = \tau_{2\beta}/\tau_{2\gamma}$). This difference in kinetics may be ascribed to the difference in cavity size between βCD and γCD. Hotarat et al. carried out a computational simulation for interaction between βCD and MGS and suggested that βCD is more suited to ingesting MGS than other CDs [19].

Summary

CDNPs encapsulated MGS as expectation. Surprisingly, CDNPs showed a higher loading ratio of MGS than native CDs. It is suggested that both the cavities of CDs and the hyperbranched polymer network in CDNPs play a critical role in the inclusion of MGS. These factors could affect the affinity between CDNPs and MGS.

Considering simple model of reaction between CD and MGS, CDNPs show almost 100 times higher CE than native CDs in binding MGS; in other words, binding constant $K_{1:1}$of interaction between CD and MGS increased 100 times by polymerization. These results are consistent with enhancement of loading ratio. Besides, it was found that (i) $K_{1:1}$ in CDNP/MGS is at the same magnitude as typical ligand-receptor interaction in biological systems. (ii) It is supposed that the reason for the enhanced binding constant may be that the ECH polymerization increases the hydrophobicity of CD rims to make it easier for MGS to enter the cavity. We also believe that the present binding constant analysis provides new insights for the application of CDNPs to novel drug delivery systems for hydrophobic drugs.

As one of the most essential issues, we studied drug release profile of MGS from CDNPs. The release of MGS can be divided into two modes: initial rapid release and second slow release. Following bi-exponential equation, in initial rapid release, just 20-25% MGS escaped from CDNPs within short time 1-2 hours (τ_1). The vast amount of MGS released from CDNPs in slow mode within longer time τ_2. We proposed model mechanism for these observations. There might be two types of CD existed in CDNPs. One is internal CD which is modified and has strong binding with MGS. The other CD is located on the surface of CDNPs which is less much modified and has less strong binding. In initial mode, MGS captured by surface CDs is released. In second mode, MGS is slowly transferred from internal CDs to surface CDs, then goes to aqueous environment.

During releasing drug, kinetical properties are considered in place of binding constant at equilibrium state. In this study, it provides that dissociation constant rate (k_d) is in inverse proportion to τ_2. The shorter τ_2 is, the larger k_d is, causing fast dissociation and short retention of capability. Therefore, despite of the similar binding affinity of β- and γCDNP against MGS in terms of binding constant, the MGS release behavior in γCDNP system was much faster than that in βCDNP. This is presumably attributable to the large k_d in the system of γCDNP due to the relatively large cavity size of the γCD structure.

Throughout Chapter III, the loading ratio, interaction with MGS and retention of capability are followed by the order: αCDNP < γCDNP < βCDNP. βCDNP seem to be the most suitable candidate carrier for MGS.

Appendix

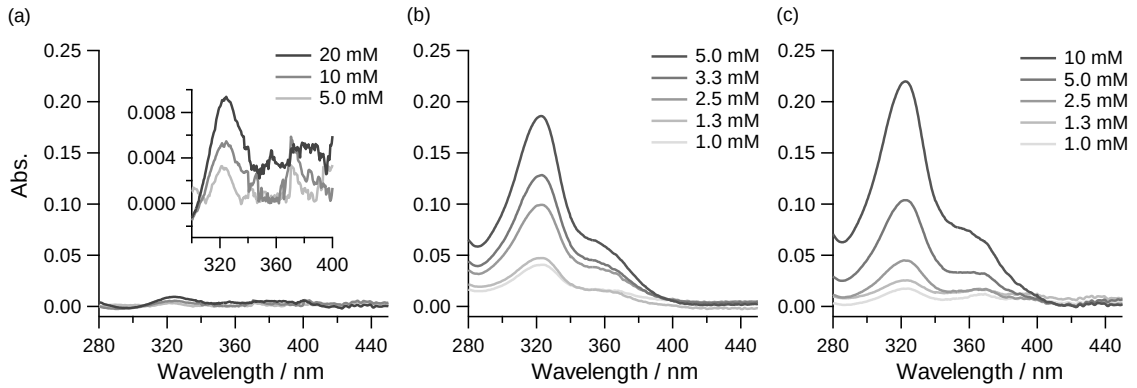

Figure 3-A1. UV-vis spectra of the complex of CD/MGS for the system of αCD (a), βCD (b), and γCD (c).

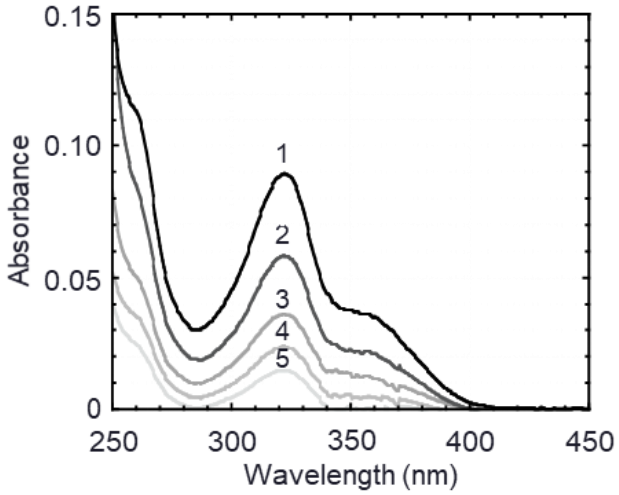

Figure 3-A2. UV-vis spectra of the complex of $\alpha CDNP_{72}$/MGS at various concentrations of $\alpha CDNP_{72}$: (1) 0.02 mM, (2) 0.01 mM, (3) 0.005 mM, (4) 0.0025 mM, (5) 0.000625 mM.

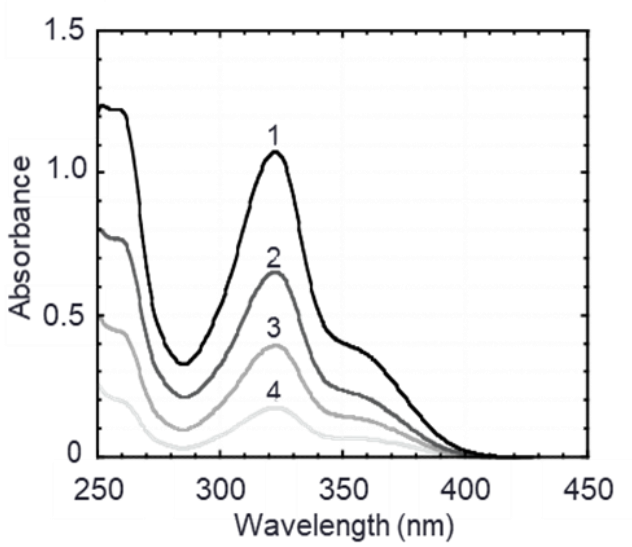

Figure 3-A3. UV-vis spectra of the complex of βCDNP$_{72}$/MGS at various concentrations of βCDNP$_{72}$: (1) 0.01 mM, (2) 0.005 mM, (3) 0.0025 mM, (4) 0.00125 mM.

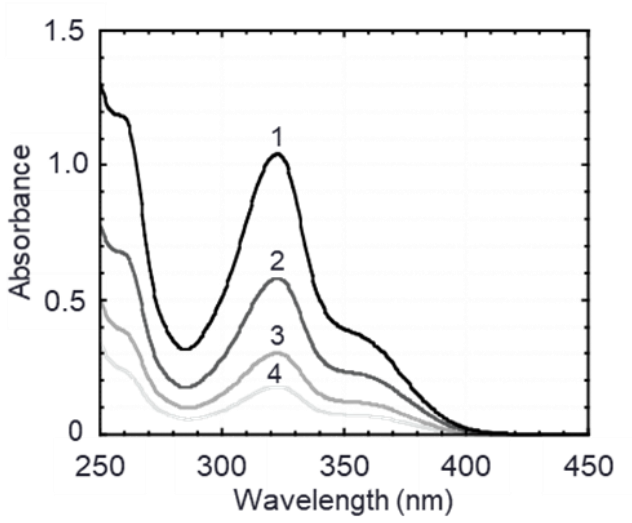

Figure 3-A4. UV-vis spectra of the complex of γCDNP$_{72}$/MGS at various concentrations of γCDNP$_{72}$: (1) 0.01 mM, (2) 0.005 mM, (3) 0.0025 mM, (4) 0.00125 mM.

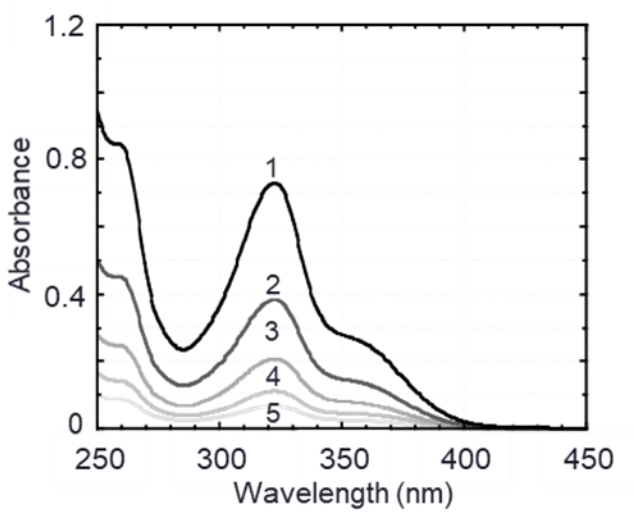

Figure 3-A5. UV-vis spectra of the complex of βCDNP$_{24}$/MGS at various concentrations of βCDNP$_{24}$: (1) 0.115 mM, (2) 0.058 mM, (3) 0.029 mM, (4) 0.014 mM, (5) 0.007 mM.

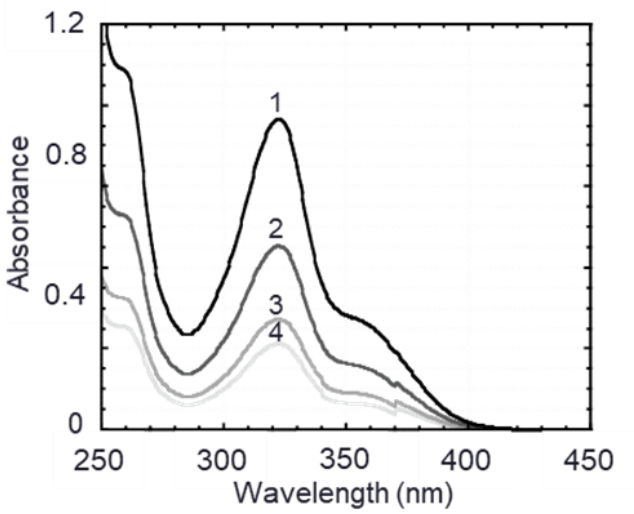

Figure 3-A6. UV-vis spectra of the complex of βCDNP$_{48}$/MGS at various concentrations of βCDNP$_{48}$: (1) 0.01 mM, (2) 0.005 mM, (3) 0.0025 mM, (4) 0.00125 mM.

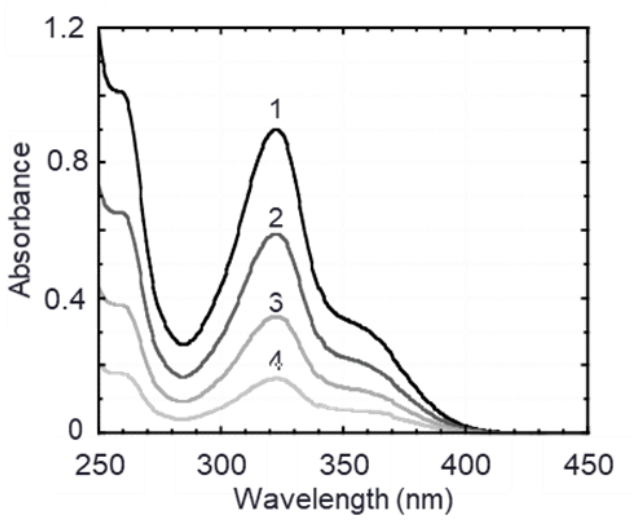

Figure 3-A7. UV-vis spectra of the complex of βCDNP$_{96}$/MGS at various concentrations of βCDNP$_{96}$: (1) 0.04 mM, (2) 0.02 mM, (3) 0.01 mM, (4) 0.005 mM.

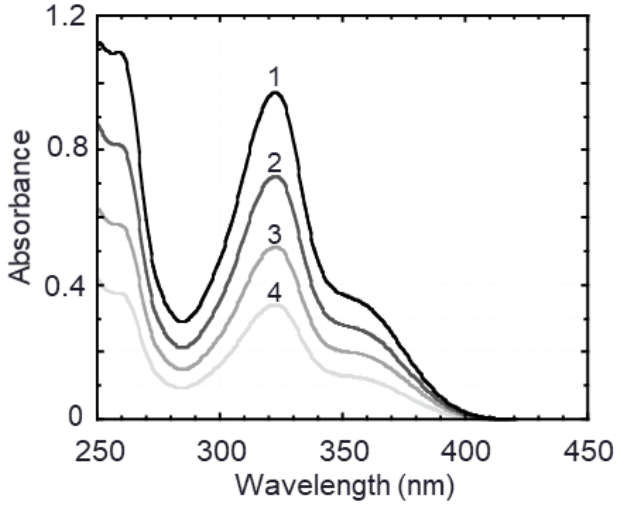

Figure 3-A8. UV-vis spectra of the complex of βCDNP$_{120}$/MGS at various concentrations of βCDNP$_{120}$: (1) 0.01 mM, (2) 0.005 mM, (3) 0.0025 mM, (4) 0.00125 mM.

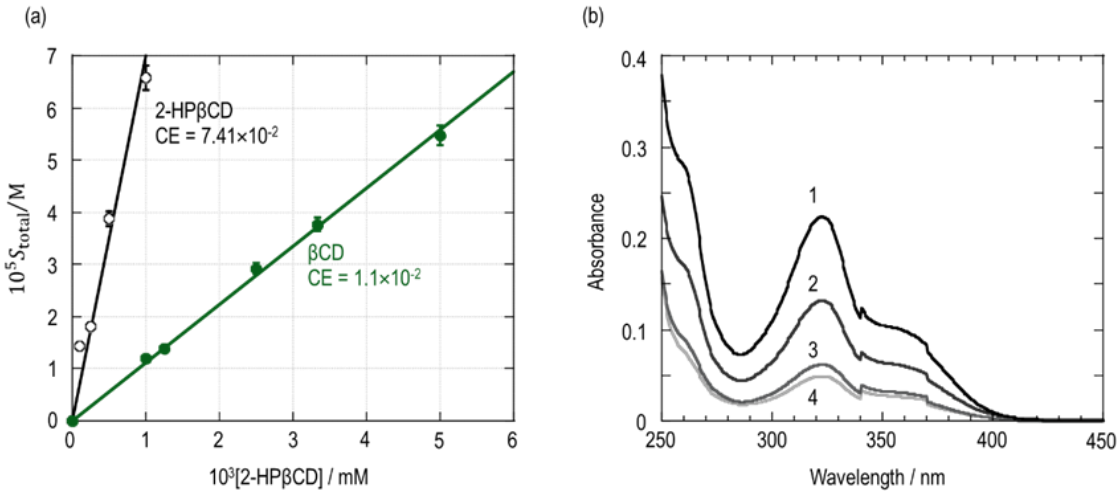

Figure 3-A9. S_{total} vs. $[\text{CD}]_t$ plot of MGS and 2-hydroxylpropyl-βCD (2-HPβCD) and its comparison with native βCD in (a). UV-vis spectra of the complex of 2-hydroxylpropyl-βCD/MGS at various concentration of 2-HPβCD in (b): (1) 1 mM, (2) 0. 5 mM, (3) 0.25 mM, (4) 0.1 mM.

Reference

1 Gidwani B. and Vyas A. A Comprehensive Review on Cyclodextrin-Based Carriers for Delivery of Chemotherapeutic Cytotoxic Anticancer Drugs. Biomed. Res. Int. 2015. 2015: 198-268. 10.1155/2015/198268.

2 Sadreraf. K., Moore E. E. and Lee M. W. Association constant of β-cyclodextrin with carboranes, adamantane, and their derivatives using displacement binding technique. J. Incl. Phenom. Macro. 2015. 83: 159-66. 10.1007/s10847-015-0552-5.

3 Higuchi T and Connors K. A Phase solubility techniques. Adv Anal Chem Instrum. 1965. 4: 117-211.

4 Jambhekar SS and Breen P. Cyclodextrins in pharmaceutical formulations II: solubilization, binding constant, and complexation efficiency. Drug Discov Today. 2016. 21: 363-68. https://doi.org/10.1016/j.drudis.2015.11.016.

5 Saokham P, Muankaew C, Jansook P and Loftsson T. Solubility of Cyclodextrins and Drug/Cyclodextrin Complexes. Molecules (Basel, Switzerland). 2018. 23: 1161-76. 10.3390/molecules23051161.

6 Couto ARS, Aguiar S, Ryzhakov A, Larsen KL and Loftsson T. Interaction of native cyclodextrins and their hydroxypropylated derivatives with parabens in aqueous solutions. Part 1: evaluation of inclusion complexes. J Incl Phenom Macro. 2019. 93: 309-21. 10.1007/s10847-018-00876-5.

7 KJ Kewal. in *Methods in Molecular Biology* Vol. 437 (ed Kewal K. Jain) Ch. 1, 1-50 (Humana Press, Totowa, NJ, 2009).

8 Wathoni N, Rusdin A, Motoyama K, Joni IM, Lesmana R and Muchtaridi M. Nanoparticle Drug Delivery Systems for alpha-Mangostin. Nanotechnol Sci Appl. 2020. 13: 23-36. 10.2147/NSA.S243017.

9 Loftsson T, Hreinsdóttir D and Másson M. The complexation efficiency. J Incl Phenom Macrocycl Chem. 2007; 57: 545-52. 10.1007/s10847-006-9247-2.

10 Yong CW, Washington C and Smith W. Structural behaviour of 2-hydroxypropyl-beta-cyclodextrin in water: molecular dynamics simulation studies. Pharmaceutical research. 2008; 25: 1092-99. 10.1007/s11095-007-9506-y.

11 Alsbaiee A, Smith BJ, Xiao L, Ling Y, Helbling DE and Dichtel WR. Rapid removal of organic micropollutants from water by a porous beta-cyclodextrin polymer. Nature. 2016. 529: 190-94. 10.1038/nature16185.

12 National Center for Biotechnology Information. PubChem Database. alpha-Mangostin,https://pubchem.ncbi.nlm.nih.gov/compound/alpha-Mangostin

13 Schibilla F, Voskuhl J, Folina NA, Dahl JEP, Schreiner PR and Ravoo BJ. Host–Guest Complexes of Cyclodextrins and Nanodiamondsasa StrongNon-CovalentBindingMotif for Self-Assembled Nanomaterials. Chemistry. 2017. 23: 16059-65. 10.1002/chem.201703392.

14 Frijlink HW, Eissens AC, Hefting NR, Poelstra K, Lerk CF and Meijer DKF. The effect of parenterally administered cyclodextrins on cholesterol levels in the rat. Pharmaceutical research. 1991. 8: 9-16.

15 Guo M, Wang X, Lu X, Wang H and Brodelius PE. α-Mangostin Extraction from the Native Mangosteen (*Garcinia mangostana L.*) and the Binding Mechanisms of α-

Mangostin to HSA or TRF. PLoS One. 2016. 11: 1-22. 10.1371/journal.pone.0161566.g001.

16 Ways JP and Parham P. The binding of monoclonal antibodies to cell-surface molecules. A quantitative analysis with immunoglobulin G against two alloantigenic determinants of the human transplantation antigen HLA-A2. Biochem J. 1983. 216: 423-32.

17 Frankel ME and Gerhard W. The rapid determination of binding constants for antiviral antibodies by a radioimmunoassay, an analysis of the interaction between hybridoma proteins and influenza virus. Mol Immunol. 1978. 16: 101-06.

18 Tobita T, Oda M and Azuma T. Segmental flexibility and avidity of IgM in the interaction of polyvalent antigens. Mol Immunol. 2004. 40: 803-11. 10.1016/j.molimm.2003.09.011.

19 Hotarat W, Phunpee S, Rungnim C, Wolschann P, Kungwan N, Ruktanonchai U, Rungrotmongkol T and Hannongbua S. Encapsulation of alpha-mangostin and hydrophilic beta-cyclodextrins revealed by all-atom molecular dynamics simulations. J Mol Liq. 2019. 288: 110965-73. 10.1016/j.molliq.2019.110965.

Chapter IV: Anticancer efficacy of CDNPs containing Alpha mangostin

IV. 1 Introduction

In chapter III, we studied the ability of encapsulating MGS. Chapter IV will present anticancer efficacy of CDNPs/MGS in both *in vitro* and *in vivo* experiment. In additional to improving MGS solubility, EPR effect is center theory for designing our nanoparticles to deliver MGS effectively to tumor. This means size of CDNP/MGS should be in range of 10-100 nm in diameter (or 5-50 nm in radius). It is convenient that we use hydrodynamic diameter in this chapter.

IV. 2 Experimental

2. 1 Dynamic light scattering (DLS)

DLS measurements for the sample solution were performed on a Beckman-Coulter DelsaMax instrument at 25°C and a scattering angle of 171°. The obtained autocorrelation function was analyzed by using the CONTIN method to obtain the hydrodynamic diameter.

2. 2 Cytotoxicity assay

The half-maximal inhibitory concentration (IC_{50}) was investigated in monolayer culture and spheroid culture of the CT26WT cell line. In brief, a total of 10^4 cells per well were seeded in a 96 well plate for 24h (in the case of monolayer culture) or 96h (in the case of spheroid culture) in a humidified incubator at 37^{o}C and, 5% CO_2. The cells were treated with various concentrations of MGS. The experiments were conducted in triplicate. Following 24h (monolayer culture) or 48h (spheroid culture) of treatment, cytotoxicity was determined using Dojindo's highly water-soluble tetrazolium salt WST-8 [2-(2-methoxy-4-nitrophenyl)-3-(4-nitrophenyl)-5-(2,4-disulfophenyl)-2H-tetrazolium, monosodium salt], which was provided with Cell Counting Kit-8 (Dojindo Molecular Technologies, Inc.). Absorbance of the formazan dye was measured using a spectrophotometer Multiskan FC (Thermo Scientific), and the results were expressed as the percentage cell viability for tumor cells. The IC_{50} was defined as the dose of agents that inhibited 50% of cell growth.

2. 3 Tumor-bearing mice

All animal procedures were performed in accordance with the Guidelines for Care and Use of Laboratory Animals of the University of Kitakyushu and approved by the Animal Ethics Committee of the University of Kitakyushu. *In vivo* anticancer activity was evaluated

using CT26WT tumor-bearing mice (the experimental schedule is shown in Figure 4-A1). First, BALB/c mice (7 weeks old, average weight ~22 g) were subcutaneously injected with 100 μL of the CT26WT cell line (10^6 cells/mice at 1:1 cell/Matrigel). The tumor volume reached ~ 100 mm^3 after 7 days of inoculation on the flank of mice. The mice were randomized into four groups of four mice each. Sample solutions (0.15 mL) were administered into the mice via intravenous (i.v.) injection. MGS was dissolved in solution containing 0.4% DMSO, 2% ethanol, and 2% Tween80 water and then administered at a dose of 10 mg/kg body weight. CDNP/MGS solutions at the MGS equivalent dose of 10 mg/kg were also i.v. injected. The tumor volume was recorded throughout the experimental period. The tumor volume (mm^3) was calculated using the formula $V = (L \times W^2)/2$, where L and W are the length and width of the tumor, respectively. Tumor growth was evaluated by the ratio of tumor volume after intravenous injection relative to that on the day of injection.

2. 4 Tissue distribution

First, βCDNP was attached with Fluorescein isothiocyanate (FITC) by the following steps: Fifty milligrams of dried βCDNP in 2 mL of DMSO was mixed with 5.5 mg of FITC. The reaction solution was kept at room temperature for 6h under dibutyl dilaurate catalysis. For purification, the reaction solution was precipitated in ethanol. After centrifugation at 100 g for 5 min at 4°C twice, the resultant precipitation was collected and dried. FITC-labeled βCDNP was used in the tissue distribution experiment.

The administration scheme for three BALB/c mice (7 weeks old, average weight ~22 g) was the same as that described in the section on "*in vivo* anticancer efficacy". At 6 h after intravenous injection, the mice were killed, and their organs and tissues were immediately removed. Weighted samples were homogenized with 1 mL of Tris-HCl buffer (50 mM, pH 8). Samples except for blood in Tris-HCl buffer were centrifuged at 12,000 g for 15 min at 4°C. In the case of blood, samples were centrifuged at 1000 g for 15 min at 4°C. Fluorescence spectroscopy of the obtained supernatant was performed using Fluoroskan FL (Thermo Scientific). The absorbance was converted into milligrams of FITC-labeled βCDNP using a calibration curve established with pure FITC-labeled βCDNP. Data are presented as milligrams of FITC-labeled βCDNP per gram of tissue.

IV. 3 Results and Discussion

3.1. Hydrodynamic diameter of CDNPs containing MGS and optimization of L_{MGS} for *in vivo* assay

The particle sizes of βCDNP and γCDNP are almost the same and about 10 nm in diameter, which is a good size for delivering particles to tumors by using the EPR effect [1]. N_{CD} is approximately the same for βCDNP and γCDNP. For αCDNP, we could not increase R_h to more than 5–6 nm, or N_{CD} to more than 20%. We suppose that the alkyl chain of epichlorohydrin was trapped by αCD during the reaction and that this interaction may have interrupted the reaction. As we found in our previous section, the binding constant between MGS and CDNP is dramatically increased by the polymerization of CD. The affinity between MGS and CD follows the order of βCD > γCD > αCD. This order is maintained after the polymerization with all of them showing increase of the binding constant by about 100 times. We are still investigating why such large enhancements occurred, but we assume that the hydrophobicity of the interior of CD in CDNPs increased because the hydroxyl groups of CDs were converted to ethers during the polymerization, which in turn increased the affinity for MGS, thus increasing the binding constant. It is safe to say that βCDNP and γCDNP are almost the same in terms of particle characters, except for the affinity to MGS.

It would be better to use CDNP/MGS particles with the maximum loading ratio of MGS because it is expected to contain highest concentration of MGS in aqueous solution. However, we found that when we used CDNPs/MGS with Max.L_{MGS}, CDNP/MGS yielded large aggregates of over 100 nm. These aggregates may be secondary aggregates of CDNP/MGS or aggregates of released MGS. Such large particles are not ideal for an *in vivo* assay because, when the drug is administered through the tail vein, the capillaries become clogged, causing the mouse to die. Before starting the bio-assay, we needed to optimize L_{MGS} so as not to create large aggregates. We dispersed CDNP/MGS into water at 10 mg/mL and left the solution to stand for a few hours, after which we subjected it to DLS. By repeating this process, we decreased L_{MGS} step by step from Max. L_{MGS}, until we did not see any large aggregates of more than 0.1 μm by DLS. This loading ratio for the *in vivo* assay is denoted as Opt.L_{MGS} . These values are 1.1% $\pm$ 0.3%, 5.3% $\pm$ 1.0%, and 4.1% $\pm$ 0.7% for αCD, βCD, and γCD, respectively. Hereinafter, we use CDNP/MGS at Opt. L_{MGS}.

Figure 4-1a shows the autocorrelation function before and after encapsulating MGS into CDNPs, where the loading wt% of MGS was set at Opt.L_{MGS}. βCDNP/MGS showed a unimodal distribution with D_h ~ 7 nm and there was no significant change in particle size between before and after the loading. Note that there was no formation of lager aggregate in βCDNP/MGS at Opt.L_{MGS}. γCDNP/MGS showed a bimodal distribution, revealing the major component with D_h ~ 11 nm and larger particles as a minor component. This minor component was present before MGS loading and we could not get rid of it by purification. Despite the presence of this component, we did not see any new large aggregate formation after loading MGS and thus decided that γCDNP/MGS could be used in further assays. For αCDNP/MGS, even when we decreased L_{MGS}<1 wt%, we observed the aggregate formation after loading MGS. This may be ascribed to the aggregation of released MGS. The binding constant between αCDNP and MGS is almost 10 times lower than that of βCDNP/MGS and γCDNP/MGS. Therefore, we can assume that MGS is more easily and rapidly released from αCDNP/MGS and aggregates in water to give new peaks around D_h ~ 170−180 nm. This is not ideal for an *in vivo* assay; however, we will evaluate it for comparison.

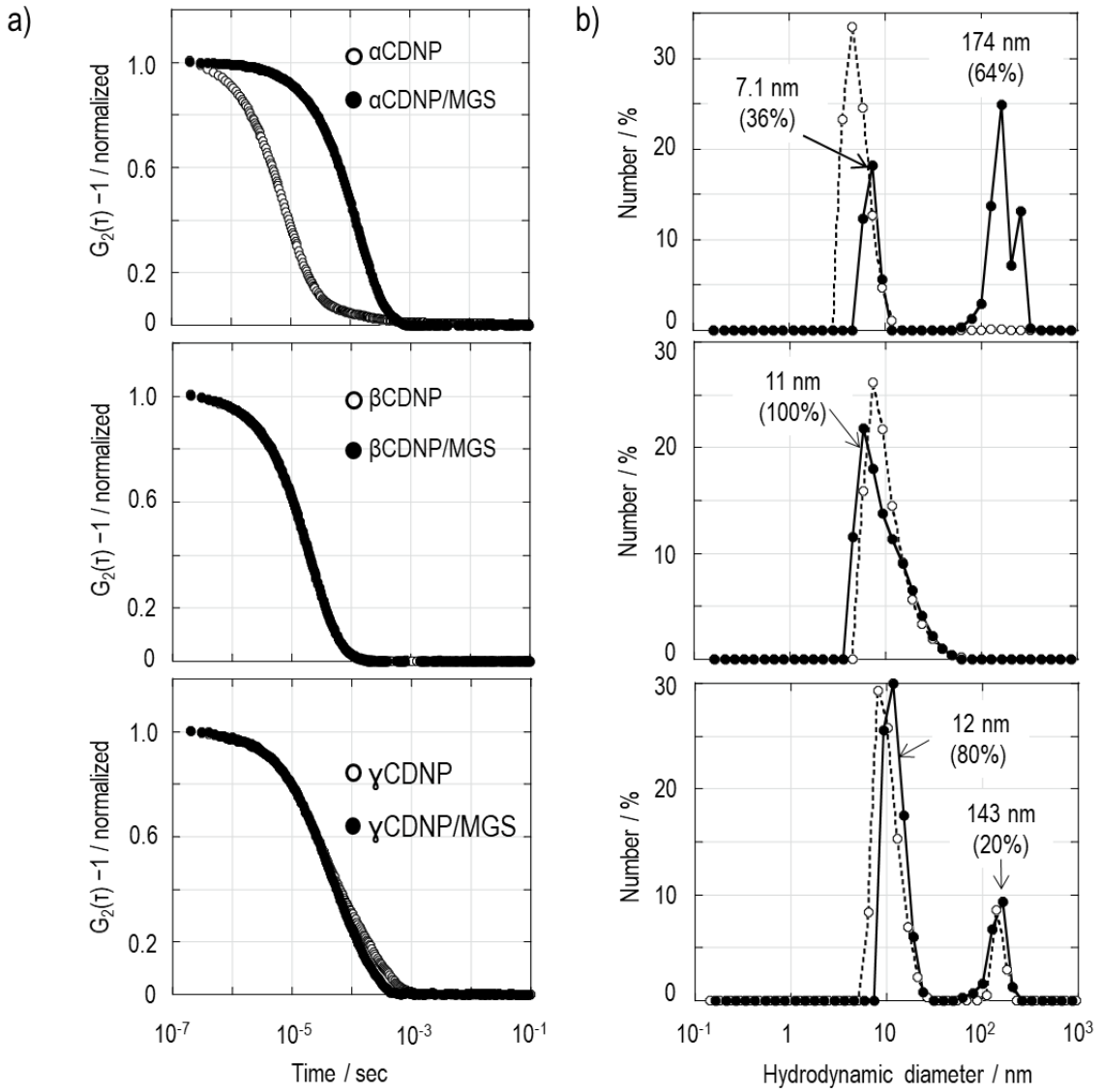

Figure 4-1. Comparison of the autocorrelation functions and the particle size distributions before (dotted line) and after (solid line) encapsulating MGS in (b).

3.2. *In vitro* experiment

Figure 4-2a plots the cell viabilities of CT26WT against the applied MGS concentration, where the viabilities were measured after 24h of incubation; the figure includes the data when βCDNP alone was applied as a negative control. The IC_{50} was determined as the MGS concentration that kills half of the cells and is summarized in Table 4-1. A smaller IC_{50} represents greater cellular toxicity. As expected, βCDNP itself was quite

harmless to the cells. The IC_{50} of MGS was ~14.5 μM and the lowest among the samples. The IC_{50} values of CDNPs/MGS were higher than that of MGS, and increased in the order of αCDNP/MGS (~27.7 μM), γCDNP/MGS (~43.5 μM), and βCDNP/MGS (~50.4 μM). This order is consistent with the retention capability of CDNPs as shown in Figure 3-5 and Table 3-4 (Chapter III). These results can be explained as follows. Once MGS is applied to the cells, it starts to kill them; therefore, naked MGS works the best. For CDNP/MGS, the MGS must first be released from the particle and thus all of the CDNP/MGS showed lower toxicity than MGS. The particles that more easily release MGS show higher toxicity; therefore, the order of the retention capability is opposite to the order of toxicity. The present findings are consistent with previous results in which drug-loaded particles were compared with the drug itself [2,3].

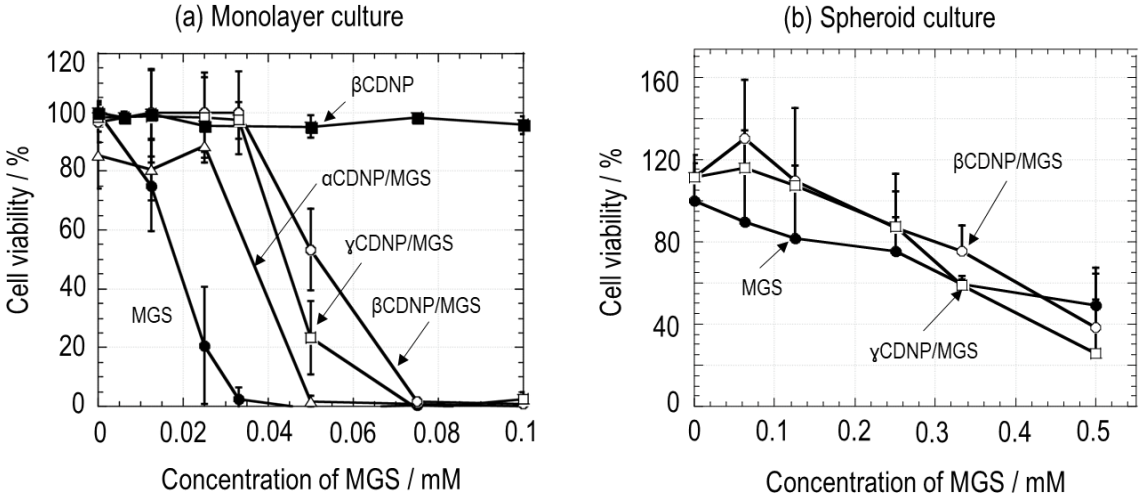

Figure 4-2. MGS concentration dependence of the cellular viability (after 24h) of monolayer (a) and spheroid (b) cultured CT26WT cells.

Table 4-1. IC_{50} Value of Free MGS and CDNPs/MGS

	Monolayer culture	Spheroid culture
MGS	14.5 ± 1.9	483.0 ± 34.9
αCDNP/MGS	27.7 ± 9.5	-
βCDNP/MGS	50.4 ± 13.2	449.6 ± 32.6
γCDNP/MGS	43.5 ± 21.0	385.0 ± 38.7

Unit is μM

We examined the MGS dose dependence for CT26WT spheroid cells, the results of which are presented in Figure 4-1b. Compared with the monolayer assays, the drug resistance was dramatically increased for all samples. IC_{50} was determined and is summarized in Table 4-1, with the data showing that IC_{50} increased about 33 times in MGS and about 9 times in CDNP/MGS. This tendency is consistent with the finding in other reports on drug-carrying nanoparticles [2,3].

Spheroid cells share similar characteristics to solid tumors in terms of their cellular heterogeneity and inter-cellular signals [4]. In contrast to the case for monolayer cells, drugs have to penetrate the cellular layers of spheroids in order to invade inside to kill the cells. In this sense, spheroid cells are also a good model for solid cancers from a drug delivery perspective. Most antitumor drugs such as pirarubicin and doxorubicin are so hydrophobic that they are easily adsorbed by the surface cells of spheroids. This causes a decrease in the drug concentration inside spheroids, which is called "drug penetration problem" [3]. It is assumed that a similar penetration problem occurs in actual solid cancer. Maeda et al. attached several pirarubicin molecules to a water-soluble polymer and diminished the hydrophobicity of the overall particle [2,5]. Their pirarubicin/polymer particle achieved better cellular penetration than pirarubicin itself. In the present study, we can assume that CDNP/MGS deeply penetrated owing to its water solubility by a similar mechanism and showed relatively high drug retention ability, which caused to better cytotoxicity and lower IC_{50} than for free MGS.

3.3. *In vivo* experiment

Figures 4-3a and 4-3b show changes in the tumor volume and tumor growth ratio after the i.v. injection of free MGS (10 mg/kg) and βCDNP/MGS at the MGS equivalent dose of 10 mg/kg into BALB/c mice bearing CT26WT tumor. Here, the tumor growth ratio is defined as the ratio of the tumor volume at the injection point relative to that at the endpoint. No notable difference was observed among the control, βCDNP, and free MGS groups. For these, the tumor volume and tumor growth ratio increased gradually over a period of 22 days and reached 1145 ± 194 nm^3 in tumor volume and tumor growth of about 10 times. Compared with these findings, βCDNP/MGS showed the considerable suppression of tumor growth. At the day 22 end point, the tumor volume was 501 ± 372 mm^3 and the tumor growth ratio was about 4. The statistical analysis indicated that there was a statistically significant difference

between these two groups. We performed a similar assay for γCDNP/MGS and found no notable difference among them as presented in Figures 4-3c and 4-3d.

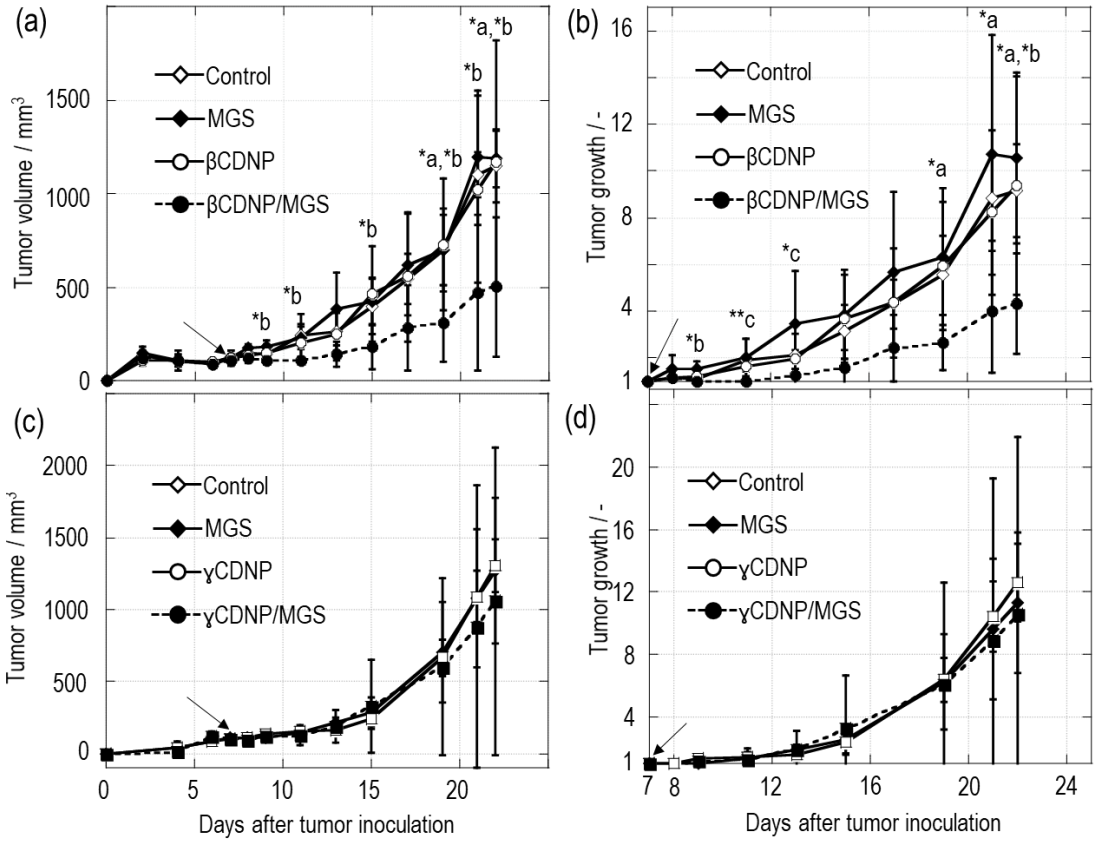

Figure 4-3. Anticancer efficacy of β- and γCDNP/MGS against CT26 tumor, compared with MGS. The tumor volumes (a, c) and the tumor growth ratios (b, d) were monitored against time after i.v. injection. Student's *t*-test was used to analyze the statistical significance of differences between the control and βCDNP/MGS group (denoted by a), MGS and βCDNP/MGS group (denoted by b), and βCDNP and βCDNP/MGS group (denoted by c). *: $p < 0.05$; **: $p < 0.01$.

MGS itself is normally rapidly cleared within 3.5h from the blood after i.v. injection with a single dose [6]. To achieve significant anticancer efficacy by using free MGS, frequent administration of MGS is required [7-9]. Shibata et al. continuously administered MGS dissolved in DMSO/ethanol (1:3 v/v) via subcutaneously implanted mini-osmotic pumps [7]. In addition, Lee et al. dissolved MGS into PBS including a small amount of DMSO and administered the solution intraperitoneally five times per week [9]. Moreover, Johnson et al. administered 100 mg/kg MGS via oral gavage five times weekly [8]. It should be noted that all of the previous works used organic solvent to increase the water solubility of MGS.

However, such use of organic solvents is not allowed in humans. Contrary to these approaches, the βCDNP/MGS in our study demonstrated anticancer efficacy via a simple single i.v. injection without any organic solvents.

Figure 4-4 (upper) shows the tissue distribution data for βCDNP, where βCDNP was marked with FITC, compared with naked FITC injection. Most of the particles remained in serum after 6h, indicating their good circulation in blood, which may have been due to the hydrophilic surface of βCDNP and the biocompatibility of CDs. Compared with FITC itself, βCDNP appeared to accumulate in the tumor, which can be explained by the EPR effect.

We can assume that both βCDNP/MGS and γCDNP/MGS were accumulated in the cancerous region with the EPR effect because both they had the same size and their other particle characters were almost the same. However, why was βCDNP/MGS much better than γCDNP/MGS in in terms of anticancer efficacy? We believe that the reason for this is difference in MGS retention ability. As illustrated in the bottom panel of Figure IV-3, after injection into blood stream, CDNP/MGS started to release MGS. This is probably occurred in a similar manner with Figure 3-5 (Chapter III). First, the MGS captured by the surface CDs was released and the releasing speed was almost the same in βCDNP/MGS and γCDNP/MGS. Later, the release was governed by the speed of transport from the internal to the surface CDs of the particle. This reflected in τ_2 and may be related to the cavity size of CDs; γCDNP/MGS has a looser cavity than βCDNP/MGS and thus the dissociation rate of γCDNP/MGS is four times faster than that of βCDNP/MGS. Therefore, we assume that MGS in γCDNP/MGS is almost completely released by the time it reaches the cancerous region, while βCDNP/MGS has some MGS left. This is the reason why βCDNP/MGS worked better. From this discussion, we can conclude that there must be an optimal range of τ_2 to achieve the best performance of MGS although we have yet to clarify this.

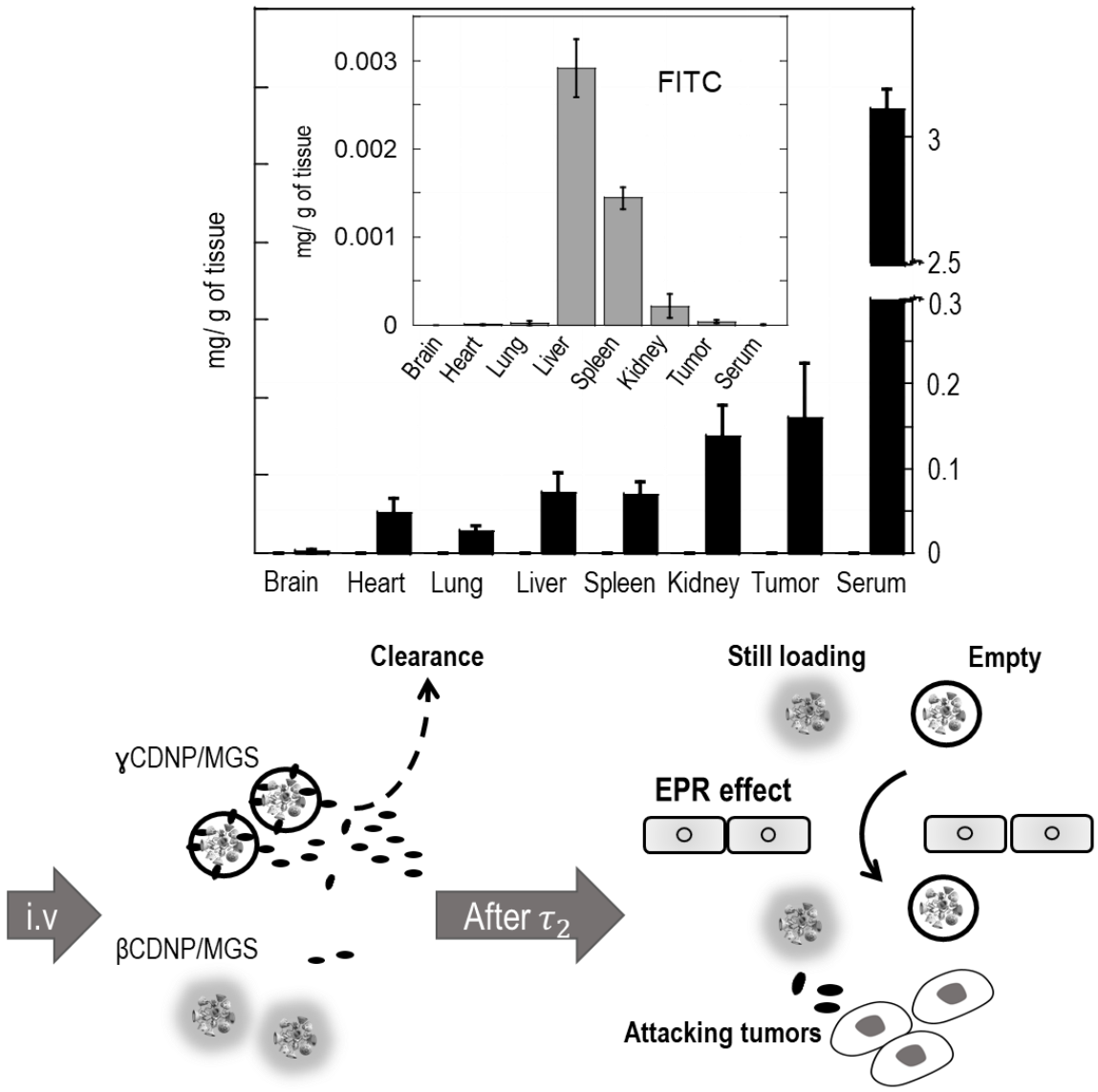

Figure 4-4. Tissue distribution of FITC (gray column) and FITC-labeled βCDNP (black column) (upper graph) and an illustration to explaining why βCDNP/MGS showed better efficacy *in vivo*.

Appendix

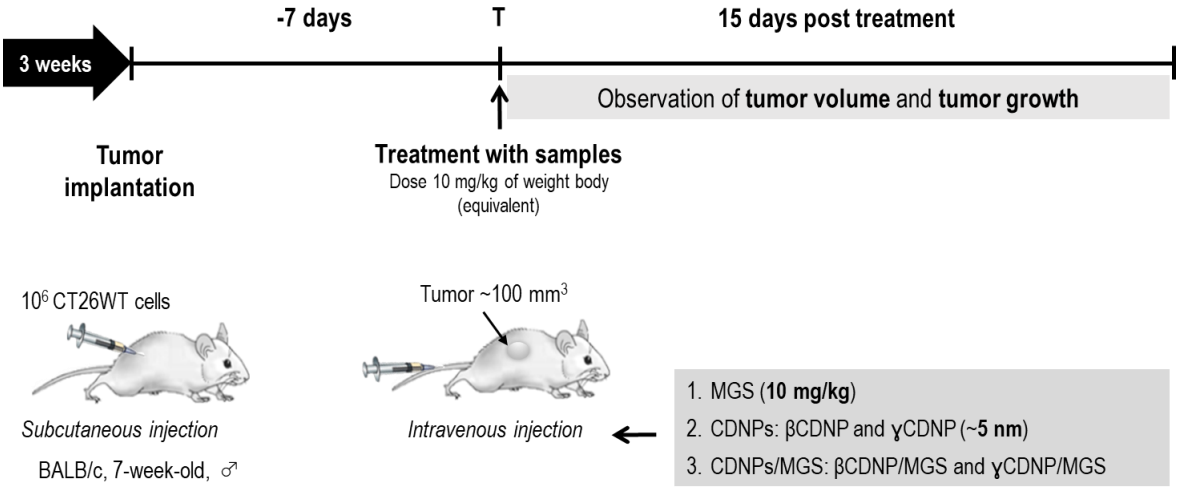

Figure 4-A1. Treatment schedule time.

References

1 Kalyane D, Raval N, Maheshwari R, Tambe V, Kalia K and Tekade RK. Employment of enhanced permeability and retention effect (EPR): Nanoparticle-based precision tools for targeting of therapeutic and diagnostic agent in cancer. Mater Sci Eng C Mater Biol Appl. 2019. 98: 1252-76. 10.1016/j.msec.2019.01.066.

2 Nakamura H, Koziolova E, Chytil P, Etrych T, Haratake M and Maeda H. Superior Penetration and Cytotoxicity of HPMA Copolymer Conjugates of Pirarubicin in Tumor Cell Spheroid. Mol Pharm. 2019. 16: 3452-59. 10.1021/acs.molpharmaceut.9b00248.

3 Lin J, Yu Y, Shigdar S, Fang DZ, Du JR, Wei MQ, Danks A, Liu K and Duan W. Enhanced antitumor efficacy and reduced systemic toxicity of sulfatide-containing nanoliposomal doxorubicin in a xenograft model of colorectal cancer. PLoS One. 2012. 7: e49277. 10.1371/journal.pone.0049277.

4 Costa EC, Moreira AF, de Melo-Diogo D, Gaspar VM, Carvalho MP and Correia IJ. 3D tumor spheroids: an overview on the tools and techniques used for their analysis. Biotechnol Adv. 2016. 34: 1427-41. 10.1016/j.biotechadv.2016.11.002.

5 Maeda H., Nakamura H. and Fang J. The EPR effect for macromolecular drug delivery to solid tumors: Improvement of tumor uptake, lowering of systemic toxicity, and distinct tumor imaging in vivo. Advanced drug delivery reviews. 2013. 65: 71-9. 10.1016/j.addr.2012.10.002.

6 Li L, Brunner I, Han A, Hamburger M, Kinghorn AD, Frye R and Butterweck V. Pharmacokinetics of a-mangostin in rats after intravenous and oral application. Mol Nutr Food Res. 2011. 55: 567-74. 10.1002/mnfr.201000511.

7 Shibata M, Iinuma M , Morimoto J , Kurose H, Akamatsu K , Okuno Y, Akao Y and Otsuki Y. a-Mangostin extracted from the pericarp of the mangosteen (Garcinia mangostana Linn) reduces tumor growth and lymph node metastasis in an immunocompetent xenograft model of metastatic mammary cancer carrying a p53 mutation. BMC Medicine. 2011. 9: 69-87. http://www.biomedcentral.com/1741-7015/9/69.

8 Johnson JJ, Petiwala SM, Syed DN, Rasmussen JT, Adhami VM, Siddiqui IA, Kohl AM and Mukhtar H. a-Mangostin, a xanthone from mangosteen fruit, promotes cell cycle arrest in prostate cancer and decreases xenograft tumor growth. Carcinogenesis. 2012. 33: 413-19. 10.1093/carcin/bgr291.

9 Lee HN, Jang HY, Kim HJ, Shin SA, Choo GS, Park YS, Kim SK and Jung JY. Antitumor and apoptosis-inducing effects of alpha-mangostin extracted from the pericarp of the mangosteen fruit (Garcinia mangostana L.)in YD-15 tongue mucoepidermoid carcinoma cells. Int J Mol Med. 2016. 37: 939-48. 10.3892/ijmm.2016.2517.

Chapter V: Summary and Conclusions

In this thesis, cyclodextrin-based hyperbranched nanoparticles (CDNPs) were created by polyaddition reaction with epichlorohydrin. Enhanced Permeation and Retention effect (EPR effect) is main theory to design our CDNPs. With CDNPs, we accomplished two main tasks that can help MGS to overcome its limitations in clinical. Among series of CDNPs, βCDNP can become a useful carrier for MGS. The following summarizes all results obtained in each chapter.

Synthesis and characterization of CDNPs (Chapter II)

Particles properties of CDNPs (molecular weight, hydrodynamic radius and CD contents) was controlled by weight ratio of Epichlorohydrin/Cyclodextrin. Only αCDNPs did not make any significant change when weight ratio increased, while the molecular weight and hydrodynamic radius of βCDNP and γCDNP increased. The size of βCDNP reached maximum peak, around 6 nm in radius that is suitable for EPR effect. At low weight ratio, epichlorohydrin just connects CDs. At higher weight ratio, it is supposed that some CDs cover the surface of CDNP to make nanoparticles water-soluble, other CDs with polymerization of epichlorohydrin are located inside of CDNPs.

The ability of encapsulating MGS in aqueous solution (Chapter III)

In Chapter III, the poor-water solubility of MGS is improved by the most use of native CDs and CDNPs. In spite of that, CDNPs encapsulated MGS with a great loading ratio of MGS than that of native CDs. It was supposed that binding constant between CD and MGS enhanced in CDNPs system. Using simple model reaction 1:1, binding constant of CD and MGS was roughly evaluated and increased 100 times by polymerization as expectation. Probably, due to converting hydroxyl group of CD to ether group during polymerization, it may be possible for MGS to easily go to cavity of CD. The interaction in CDNPs system was considered to be at the same level of antigen-antibody interaction. Among CDNPs, βCDNP gave the best for loading ratio as well as binding constant compared with α- and γCDNP.

As a matter of using nanoparticle in drug delivery system, drug release profile was also monitored to understand how CDNPs release MGS. All α-, β-, and γCDNP showed two modes: initial rapid release and second slow release. According to Chapter II, there may be two types of CD: internal CDs and surface CDs. These CDs differ from affinity with MGS.

Internal CDs have more strong binding with MGS than surface CDs. Thus, we proposed a model of releasing MGS from CDNPs. Most of MGS may be kept in internal CDs and released in second slow mode. Before going to outside, MGS escapes from internal CDs, then is transferred to surface CDs. In complex with surface CDs, MGS will rapidly release into environment.

In contrast to encapsulation, kinetical properties are considered in releasing MGS instead of binding constant. It can provide a relationship between lifetime of CDNP/MGS (τ_2) in second slow mode and dissociation constant rate (k_d). k_d is in inverse proportion to τ_2. The τ_2 of βCDNP/MGS is longer than that of γCDNP/MGS, so the dissociation reaction in βCDNP/MGS complex occurs fast than that in γCDNP/MGS complex, ~4 times. The cavity size of CD might be a reason for this difference in terms of k_d.

Anticancer efficacy of CDNPs/MGS (Chapter IV)

We presented anticancer efficacy of CDNP containing MGS in Chapter IV. All CDNPs containing MGS showed cytotoxicity *in vitro* but only βCDNP/MGS suppressed tumor volume and tumor growth *in vivo*. It is demonstrated that βCDNP accumulated in tumor as a result of EPR effect. More importantly, EPR effect appears to be insufficient to explain the lack of anticancer efficacy in case of γCDNP/MGS. Although many studies have been performed to develop better carriers for delivering hydrophobic drug compounds, to the best of our knowledge, there are no basic principles to design such carriers, except for their size in terms of the EPR effect. In the present work, it is proposed that the drug retention time or τ_2 seem to be for such design. The best τ_2 may differ depending on the particular cancer and drug, but this principle may be universal across all hydrophobic drugs.

List of publication

Part of this thesis has been or will be published in the following papers

1. Cyclodextrin-Based Nanoparticles Encapsulating α-Mangostin and Their Drug Release Behavior: Potential Carriers of α-Mangostin for Cancer Therapy

   Van T. H. Doan, Ji Ha Lee, Rintaro Takahashi, Phuong T. M. Nguyen, Van Anh T. Nguyen, Huong T. T. Pham, Shota Fujii, and Kazuo Sakurai

   Polymer Journal 2020, 52(4), p.p. 457–466

2. Enhanced Binding Constant of Cyclodextrin to Alpha-mangostin in Hyperbranched Polymers

   Doan Thi Hong Van, Doan Thi Ngoc Anh, Shota Fujii, and Kazuo Sakurai

   Chemistry Letters 2020. DOI: https://doi.org/10.1246/cl.200210 (just accepted)

3. Anticancer Efficacy of Cyclodextrin-Based Hyperbranched Polymer Nanoparticles Containing Alpha-Mangostin

   Van T. H. Doan, Shin Takano, Ngoc Anh T. Doan, Phuong T. M. Nguyen, Van Anh T. Nguyen, Huong T. T. Pham, Koji Nakazawa, Shota Fujii, and Kazuo Sakurai

   Submitted to Polymer Journal

Other related work:

1. Patent 2019-172063

   Kazuo Sakurai, Shota Fujii, Doan Thi Hong Van, Nguyen Thi Mai Phuong, Nguyen Thi Van Anh, Pham Thi Thu Huong